External application of human umbilical cord-derived mesenchymal stem cells in hyaluronic acid gel repairs foot wound of type I and type II diabetic rats through paracrine action mode

Jingan Chen
Zhejiang Chinese Medical University
Yi Liu
Zhejiang Chinese Medical University
Jingwen Zhang
Zhejiang Chinese Medical University
Haowei Liang
Zhejiang Chinese Medical University
Ting Li
Zhejiang Chinese Medical University
Li Yan
Zhejiang Chinese Medical University
Li Zhou
Zhejiang Chinese Medical University
Letian Shan
Zhejiang Chinese Medical University
Hui Wang (wh@zcmu.edu.cn)
Zhejiang Chinese Medical University https://orcid.org/0000-0003-0108-8254

Research Article

Keywords: Diabetic foot ulcer, External application, Human umbilical cord-derived mesenchymal stem cells, Hyaluronic acid gel, Wound healing, Paracrine

Posted Date: May 16th, 2022

DOI: https://doi.org/10.21203/rs.3.rs-1638337/v1

Abstract

Background: Diabetic foot ulcer (DFU) is a main complication of diabetes mellitus with high rate of amputation and low rate of therapeutic success. External application of mesenchymal stem cells (MSCs) provides a new therapeutic option to treat DFU and avoids the drawbacks of injective MSCs therapy. In this study, human umbilical cord-derived MSCs-hyaluronic acid gel (hucMSCs-HA gel) was developed for evaluating the external efficacy of MSCs on DFU, and its paracrine mode of action was explored by using hucMSCs-conditional medium (MSC-CM).

Methods: *In vivo*, type I and type II diabetic rat models were established and received hucMSCs-HA gel external treatment, and histopathological staining (HE and Masson) and immunohistochemical analysis were conducted. *In vitro*, human umbilical vein endothelial cells (HUVECs) and human skin fibroblasts (HSFs) were exposed to high glucose and received MSC-CM treatment, and the assays of cell viability, wound healing, transwell migration, tube formation, cell senescence, reactive oxygen species (ROS), malondialdehyde (MDA) detection, qRT-PCR, and Western blot were conducted. The *in vivo* data indicated that hucMSCs-HA gel accelerated DFU healing in both type I and type II diabetic rats by improving re-epithelialization, collagen deposition, and angiogenesis, in which hucMSCs played a major role in the gel.

Results: The *in vitro* data demonstrated that MSC-CM not only improved cell viability, wound healing, migration, tube formation, and cell senescence of HUVECs, but also promoted cell viability, accelerated wound healing, and reduced ROS and MDA production of HSFs, suggesting a paracrine mode of action of hucMSCs in treatment of DFU. Moreover, MSC-CM significantly restored the abnormal expressions of pro-inflammatory and antiangiogenic genes (*TNF-α*, *IL-1β*, *IL-6*, *ET-1* and *p16*) and proliferative protein (PCNA) of HUVECs, and also restored the pro-fibrotic and antioxidant genes (*COL1A1*, *COL3A1*, *COL4A1*, *SOD1* and *SOD2*) and proteins (PCNA and COL1) of HSFs.

Conclusions: These results suggested that hucMSCs-HA gel facilitated DFU healing of type I and type II diabetic rats mainly through paracrine actions on HUVECs and HSFs. This study provided new insights into MSCs therapy and a promising therapeutic strategy for the clinical treatment of DFU.

Background

Diabetes mellitus is a globally severe condition accompanied with the rapidly increasing incidence (projected 12.2% by 2045) and large health expenditures (projected $1,054 billion by 2045) [1]. As the diabetes pandemic progresses, diabetic foot ulcer (DFU) becomes a major diabetic complication with high mortality and disability rates, which massively decreases life quality of patients and increases healthcare costs [2, 3]. DFU refers to full-thickness foot wound affecting dermal tissue and vessels located below the ankle in a diabetic patient, and is related to diabetic neuropathy and peripheral arterial disease [4]. About 9.1 to 26.1 million people develop DFU, and 85% of them suffered limb amputations, along with the morbidity of 6.23% (type I diabetes) and 6.72% (type II diabetes) [5]. The conventional management of DFU is standard wound care with debridement, followed by antibiotics and dry dressings,

which fails to induce tissue regeneration and remodeling, but always results in antimicrobial resistance and secondary ulceration [6, 7]. Dry dressings (gauze, cotton pads, and bandages) are widely used for DFU treatment, but their shortcomings are outstanding, such as difficulty in keeping wound bed moist and adhesion to granulation tissue [8, 9]. Recently, many adjunctive therapies have been developed and brought hope, including bioengineered skin grafts, hyperbaric oxygen therapy, negative pressure wound therapy, and biomaterial dressings [10]. However, these therapies have limitations, e.g., xenograft or artificial skin grafts have low bioavailability or produce immune rejection [11], and hyperbaric oxygen and negative pressure rely on special infrastructure, prone to barotrauma complications and increase bacterial infection rate [12, 13]. Biomaterials, such as collagen, chitosan, and hyaluronic acid (HA) gel, are inexpensive and provide a moist wound healing environment, benefiting epithelialization and autolytic debridement [14]. However, without seed cells, the wound repair effects of these gels remain unsatisfactory [15]. Combination of seed cells and biomaterial gel would be a promising strategy for wound healing treatment of DFU, attracting increasing attentions.

Mesenchymal stem cells (MSCs) are a type of pluripotent progenitor cells with high self-renewal, differentiation, tissue regeneration, and immune regulation abilities, which can be isolated from various human tissues, such as umbilical cord, adipose tissue, and bone marrow, etc [16, 17]. Currently, MSCs become an important source of cell-based therapies for various diseases, such diabetes [18]. Clinical trials indicated that bone marrow-derived MSCs could effectively improve insulin sensitivity and C-peptide response in type II diabetic patients [19]. Zhou et al observed that umbilical cord-derived MSCs transplantation delayed hyperglycemic progression, prevented weight loss, and doubled serum insulin and C-peptide levels in type II diabetic rats, and found that the MSCs exerted trophic effects on islets, improved the islet viability and insulin secretion by secreting β-cell growth factors (IGF-1, HGF, and PDGFA) [20]. Nowadays, with the widespread use of MSCs in diabetes, there is growing attention on the treatment of diabetic complications, especially DFU [21, 22]. A clinical trial was conducted, in which hyaluronic acid (HA) gel loaded with adipose-derived MSCs were applied to treat DFU of diabetic patients and showed better wound closure rate (82%) and Kaplan-Meier median closure time (28.5 days) than control rate (53%) and closure time (63.0 days) [23]. Paracrine has been found as a main action mode of MSCs for wound repair, which increases epithelialization, granulation tissue formation and angiogenesis by paracrine pathways [24, 25]. For instance, intravenously transplantation of umbilical cord-derived MSCs secreted growth factors (VEGF, bFGF and HGF) that promoted angiogenesis and collagen deposition, thereby regulating inflammation in wound tissue and accelerating wound healing in diabetic rats [26]. To date, the mainstay of MSCs therapy studies for DFU focused on the injection route (intravenous injection, intravenous infusion, or topical injection). Although the injection of MSCs achieved therapeutic effects, its limitations also gradually emerged, such as inconvenient operations, unknown risk of rejection reaction of allogeneic MSCs transplantation, and secondary damage on skin caused by the syringe needle (topical injection) [27]. Currently, few attentions have paid on the external application of MSCs for DFU treatment.

To fill the above gaps, this study developed an external therapy approach of MSCs by using HA gel to treat DFU. Human umbilical cord-derived MSCs (hucMSCs) was applied to prepare hucMSCs-HA gel, in

which hucMSCs played a leading role and HA gel was utilized as a drug carrier to maintain cell activity and prolong functional time of hucMSCs. The hucMSCs-HA gel was directly covered on the DFU wound of both type I and II diabetic rat models, and human umbilical vein endothelial cells (HUVECs) and human skin fibroblasts (HSFs) were used to evaluate the paracrine effects of hucMSCs-HA gel. This study firstly applied hucMSCs-HA gel to treat DFU through direct external way, which overcame the limitations of MSCs injection and indicated application potential in the treatment of DFU.

Materials And Methods

Chemicals and reagents

Streptozotocin (STZ) was obtained from Sigma (Saint Louis, USA). Sodium hyaluronate powder was purchased from Shanghai yuanye Bio-Technology Co., Ltd (Shanghai, China). Alpha-minimum essential medium (α-MEM) was purchased from Gibco BRL (NY, USA). Dulbecco's modified Eagle's medium (DMEM) was purchased from Zhejiang Senrui Biotechnology Co., Ltd. Trypsin (0.25%) was purchased from Biosharp (Beijing, China). Fetal bovine serum (FBS) was purchased Gibco (Auckland, New Zealand). 3-(4,5)-dimethylthiahiazo(-z-y1)-3,5-di-phenytet-razoliumromide (MTT) was purchased from Sigma-Aldrich, USA. Cell culture plates were purchased from Thermo Fisher Scientific Inc. (Waltham, MA, USA). Transwell chambers and Matrigel® Growth Factor Reduced Basement were purchased from Corning (NY, USA). The Malondialdehyde (MDA) Detection Kit was purchased from Nanjing Jiancheng Bioengineering Institute (Nanjing, China). TRIzol reagent was obtained from Thermo Fisher Scientific, Inc. (MA, USA). The miScript SYBR Green PCR kit was obtained from Qiagen (Dusseldorf, Germany). Senescence β-Galactosidase Staining Kit (C0602), RIPA buffer, BCA Protein Assay Kit and Reactive Oxygen Species Assay Kit were purchased from Beyotime Institute of Biotechnology (Jiangsu, China). The antibodies (anti-PCNA, anti-COL1, anti-VEGFA, and anti-β-ACTIN) were purchased from Novus Biologicals, Inc. (Littleton, USA) and horseradish peroxidase–conjugated antibody was purchased from Zhongshan Jinqiao Biotechnology Co., Ltd (Beijing, China).

Cell culture and flow cytometry identification of hucMSCs

In this study, hucMSCs were obtained from Cell Resource Bank and Integrated Cell Preparation Center of Xiaoshan (Hangzhou, China) and incubated in α-MEM containing 10% FBS, L-glutamine, ribonucleosides, deoxyribonucleosides at 37 °C, 5% CO_2. To ensure the accuracy of subsequent experiments, flow cytometry analysis was applied to identify the biological properties of hucMSCs. Firstly, hucMSCs were seeded into 10 cm dishes under the above culture condition, grown to 80% ~ 90% confluence, passaged 3 - 4 generations and then collected at cell density of 1×10^9 cells per tube. Secondly, CD34-FITC, CD45-FITC, HLA-DR-FITC, CD73-FITC, CD90-FITC, and CD105-APC antibodies were added for incubation at 4 °C in dark for 30 min, respectively. Finally, positive rates of these surface markers of stem cells were tested by Accuri C6 flow cytometer (BD Biosciences, San Jose, CA, USA).

Preparation of hucMSCs-HA gel (MSC-HA)

In preparation of MSC-HA, HA (USP, 1000 – 1500 kDa) was applied as a scaffold for hucMSCs in the treatment of DFU. Sodium hyaluronate powder (24 mg) was dissolved in 3 ml PBS (8 mg/ml) to prepare HA-based spongy gel at room temperature. Before the gel solidification, 3×10^6 hucMSCs were mixed with the gel to prepare the hucMSCs-HA gel (MSC-HA) (1×10^6 cells/ml).

Animals

Male Sprague Dawley (SD), Wistar and Goto-Kakizaki (GK) rats were purchased from SLAC Laboratory Animal Co. Ltd (Certificate No: SCXK (Shanghai) 2017-0005). Among them, SD rats (eight weeks old, 250-280 g) were used to establish type I diabetic model, and GK rats (12 weeks old, 300-350 g) were used to establish type II diabetic model. All rats were fed in SPF animal room with standard environmental conditions (22 ± 2 °C, relative humidity of 55 ~ 60%, and 12 h light / 12 h dark cycles). All animal experiments were approved by the Animal Ethics Committee of Zhejiang Chinese Medical University, Hangzhou, China and met the guidelines for the Care and Use of Laboratory Animals published by the National Institutes of Health Animal (Ethics No: 11410).

Type I diabetes modeling

A total of thirty-two SD rats were applied in type I diabetes modeling and four experimental groups were set as follow: (i) control group, (ii) type I diabetic model (T1DM) group, (iii) HA treatment (HA) group, and (iv) hucMSCs-HA gel treatment (MSC-HA) group. In modeling, twenty-four SD rats were administrated by freshly prepared STZ in citrate buffer (dissolved in 0.1 mM citrate buffer, pH 4.2 ~ 4.5) at a dosage of 50 mg/kg by tail vein injection, and eight SD rats received an equal volume of citric buffer as control group. After STZ administration for 7 days, SD rats with blood glucose level ≥ 16.1 mM were selected as type I diabetic rats and randomly divided into three groups (T1DM, HA, and MSC-HA). The HA group and MSC-HA group were treated with HA gel and hucMSCs-HA gel, respectively.

Type II diabetes modeling

In establishment of type II diabetic rat model, ten Wistar and twenty GK rats were used and four groups were set as follow: (i) control group, (ii) type II diabetic model (T2DM) group, (iii) HA treatment (HA) group, and (iv) hucMSCs-HA gel treatment (MSC-HA) group. In modeling, the control group consisted of Wistar rats, moreover, according to the previously described characteristics of the adult GK rats [28, 29], GK rats with blood glucose level of 10-20 mM were selected as type II diabetic rats and randomly divided into three groups (T2DM, HA, and MSC-HA). The HA group and MSC-HA group were treated with HA gel and hucMSCs-HA gel, respectively.

Dorsal foot skin wound modeling of type I and II diabetic rats

After successful establishment of all experimental groups in type I and type II diabetes modeling, the full-thickness dorsal skin wounds (5 × 10 mm) of both feet of all rats in experimental groups above were surgically created to establish DFU wound models. Digital images of all diabetic foot wounds were taken

every three days until the wound in the control group healed completely, and the foot wound area (mm^2) was quantified using Image-J software (Version 1.49, National Institutes of Health, Bethesda, USA). To reflect the change in wound area from the original area, the average wound surface healing rate was calculated by the formula = (sq.0 – sq.A) / sq.0 × 100%, where sq.0 represented the average original wound area on day 0, and sq.A represented the wound area on day A. After treatment, foot skin samples were obtained from euthanized diabetic rats, bisected through the center of the lesion to obtain the largest diameter of the wound, and then fixed in 4% paraformaldehyde for further experiments.

Histopathological and immunohistochemical staining

In order to evaluate the therapeutic effect of hucMSCs on diabetic foot, the pathological features, collagen deposition and angiogenesis were analyzed by HE staining, masson staining and immunohistochemical experiments, respectively. Firstly, all foot skin samples were dehydrated and embedded in paraffin using the Thermo Scientific Excelsior AS (ThermoFisher Scientific Inc., MA, USA) and Thermo HistoStar (ThermoFisher Scientific Inc., MA, USA), respectively. Secondly, 4 μm sections of skin paraffin-embedded samples were cut through Semi Motorized Rotary Microtome RM2245 (Leica, Wetzlar, Germany). Thirdly, HE staining was performed by ST5010 Autostainer (Leica, Wetzlar, Germany), and masson staining by Masson's Trichrome Stain Kit (G1340, Solarbio, China). For immunohistochemistry, sections were deparaffinized, rehydrated, and then retrieved with heat-induced epitope retrieval. Endogenous peroxidase was inhibited with 3% hydrogen peroxide. The slides were then incubated with the primary antibody (anti-VEGFA, dilution 1 : 50) overnight, rinsed 3 times in phosphate-buffered saline (PBS) for 5 min at room temperature, and incubated with a biotinylated secondary antibody (dilution 1 : 100) for 1 h, rinsed 3 times in PBS at room temperature. Immunohistochemical detection was performed with 3,3'-diaminobenzidine tetrahydrochloride (DAB). Fourthly, all sections from HE, masson, and immunohistochemical staining were sealed with neutral gum and photographed using a Nikon Eclipse 80i microscope (Nikon, Tokyo, Japan). Finally, quantitative analyses of Masson's Trichrome (collagen deposition) and immunohistochemistry (VEGFA staining density and number of blood vessels) were performed using Image-J software (Version 1.49, National Institutes of Health, Bethesda, USA) and the Image-Pro Plus software (Version 6.0, Media Cybernetics, Silver Spring, USA), respectively.

Cell culture of HUVECs and HSFs

HUVECs and HSFs were purchased from the Chinese Academy of Sciences (Beijing, China). At 37 °C, 5% CO_2 and humidified atmosphere, both HUVECs and HSFs were cultured in DMEM with 25 mM glucose, 10% FBS, 100 U/ml penicillin and 100 μg/ml streptomycin. After the cell confluence reached approximately 80%, cells were digested with 0.25% trypsin, passaged 3–6 times, and then applied for the follow-up experiments.

Conditioned medium preparation of hucMSCs, HUVECs and HSFs

HucMSCs were seeded into 10 cm dishes and grown to 80% ~ 90% confluence in α-MEM. After the removal of supernatant, hucMSCs were washed three times with PBS and DMEM (25 mM glucose) was

added into the dishes for 48 h. Next, the supernatant was centrifuged at 1000 rpm for 10 min to remove cell debris and collected as the conditioned medium of hucMSCs (MSC-CM). Moreover, the conditioned medium of HUVECs (HUVEC-CM) and HSFs (HSF-CM) were also prepared using DMEM (25 mM glucose) as above and utilized as the parallel control for MSC-CM, so that the medium would not affect the outcome.

Cellular experimentation and MSC-CM treatment

To mimic diabetic condition and investigate the therapeutic effect and mode of hucMSCs in vitro, both HUVECs and HSFs were cultured in high glucose (HG) and then treated with MSC-CM in our study. Three experimental groups in these two types of cells were separately established, including the control group cultured in normal medium (25 mM glucose), the model (HG) group cultured in high glucose (50 mM glucose), and the MSC-CM group cultured in high glucose (50 mM glucose). In cellular modeling, HUVECs and HSFs were incubated in high glucose environment for 48 h. Then during treatment for another 48 h, on one hand, HUVECs from the control and HG groups were cultured in HUVEC-CM, while those from MSC-CM group in the MSC-CM, on the other hand, HSFs from the control and HG groups were cultured in HSF-CM, while those from MSC-CM group in the MSC-CM. After treatment, HUVECs and HSFs from their control, HG and MSC-CM groups were applied for the following experiments.

Cell viability assay

To evaluate the effect of hucMSCs on the viability of HUVECs and HSFs, HUVECs and HSFs were seeded at a density of 3000 cells per well in 96-well plates, and treated with different glucose concentrations and MSC-CM as described above. Subsequently, HUVECs and HSFs were added with 50 μl MTT solutions, and incubated for 4 h at 37 °C in the dark. After all supernatants were removed, 150 μl dimethyl sulfoxide (DMSO) each well was added into HUVECs and HSFs, shaking for 10 min and dissolving the purple formazan formed by the reduction of MTT. Finally, the measurement of optical density (OD) values per well was detected at a wavelength of 490 nm (HUVECs) and 570 nm (HSFs) using the microplate photometer (Multiskan™ FC, ThermoFisher Scientific Inc., Waltham, MA, USA).

Wound healing assay

Here, the horizontal migration capabilities of HUVECs and HSFs were assessed by wound healing assay. 2 ml cell suspensions of HUVECs (3×10^4 cells/ml) and HSFs (4×10^4 cells/ml) were separately seeded in the 6-well plates, treated with different glucose concentrations and MSC-CM as described above, and cultured to ~ 100% confluence in each well. Then, the scratch cell-free zone was manually created across the cell monolayer by a sterile 10 μl pipette tip. The cells were subsequently washed twice with PBS to remove cellular debris and cultured for 24 h in fresh DMEM medium. After scratching, HUVECs and HSFs migration were observed and photographed using an inverted microscope (Carl Zeiss, Gottingen, Germany), and the wound area was calculated with the Image-J software (Version 1.49, National Institute of Heath, Bethesda, USA). The wound closure percentage was obtained by the following formula: wound

closure rate (%) = $(A_0 - A_t) / A_0 \times 100$, where A_0 was the wound area at 0 h and A_t was the remaining area at the designated time.

Transwell migration assay

To detect the vertical migration capability of HUVECs, transwell migration assay was performed. Firstly, 3×10^4 cells/well HUVECs were seeded in 6-well plate and exposed to various glucose concentrations and MSC-CM as described above. After treatment, HUVECs were digested by trypsin and then 4000 cells/well were re-seeded in the upper chamber of 24-well transwell plate with a polycarbonate membrane. Cultured in serum-free DMEM medium for 15 h, the upper chamber was gently wiped and HUVECs migrated to the underside were fixed with 4% paraformaldehyde and stained with haematoxylin and eosin. Finally, the migrated HUVECs were observed and photographed on four random microscope fields (× 200) using the FLEXACAM C1 microscope (Leica, Wetzlar, Germany), and migrated cell number was calculated by Image-J software (Version 1.49, National Institutes of Health, Bethesda, USA).

Reactive oxygen species (ROS) production and lipid peroxidation determination

To evaluate the generation of high glucose-mediated oxidative stress in HSFs, intracellular ROS level was measured using the Reactive Oxygen Species Assay Kit (S0033S). HSFs were seeded in a 24-well plate with 4000 cells/well, cultured in different glucose concentrations and treated with MSC-CM as described above. Following the manufacturer's instructions, cells were washed twice with PBS and incubated in serum-free medium with 10 μmol/L oxidation-sensitive fluorescent probe (dichloro-dihydro-fluorescein diacetate, DCFH-DA) at 37 ºC for 20 min. Subsequently, cells were washed three times with serum-free medium and observed under a Zeiss microscope (Carl Zeiss, Gottingen, Germany). Four random fields per well were captured by Zen software (Carl Zeiss, Gottingen, Germany) and then ROS fluorescence intensity was calculated by Image-J software (Version 1.49, National Institutes of Health, Bethesda, USA).

For lipid peroxidation determination, MDA (a marker of lipid peroxidation) level of HSFs supernatant was determined using the Malondialdehyde (MDA) Detection Kit (A003-1-2) based on thiobarbituric acid (TBA) reactivity. Briefly, 8×10^4 cells/well HSFs were seeded in 6-well plate and cultured as above. After treatment, HSFs supernatants were collected and mixed with TBA, reacting at 90–100 °C and acidic condition according to the manufacturer's protocols. Finally, MDA level was measured at 532 nm using the microplate photometer (Multiskan™ FC, ThermoFisher Scientific Inc., Waltham, MA, USA).

Cell senescence staining

To observe the effect of MSC-CM on the aging phenomenon of HUVECs, cell senescence assay was performed by senescence-associated galactosidase (SA-β-Gal) staining using Senescence β-Galactosidase Staining Kit (C0602). In brief, HUVECs were seeded in 6-well plates with 4×10^4 cells/well and treated with different glucose concentrations and MSC-CM as above. According to the manufacturer's instructions, HUVECs were rinsed twice with PBS, added with fixative for 15 min, washed twice with PBS, and subsequently stained with working solution of β-galactosidase with X-Gal at 37 °C

for 2 h. Finally, the proportion of SA-β-galactosidase cells in five randomly selected microscope fields (× 400) obtained from a Zeiss microscope (Carl Zeiss, Gottingen, Germany) was calculated by Image-J software (Version 1.49, National Institutes of Health, Bethesda, USA).

Tube formation assay

To explore the role of MSC-CM in the angiogenesis of HUVECs, tube formation assay was carried out using Matrigel® Growth Factor Reduced Basement. Firstly, HUVECs (4×10^4 cells/well) were seeded into s6-well plate and then treated with different glucose concentrations and MSC-CM as described above. Secondly, following the treatment, 50 μl of growth-factor reduced Matrigel per well was added into pre-coated 96-well plate and solidified at 37 °C for 30 min. Thirdly, HUVECs were collected after trypsin digestion and 1000 cells were re-seeded into the pre-treated 96-well plate with solidified Matrigel. Cultured at 37 °C for 4 h, the tube network formation was observed under an inverted microscope (Carl Zeiss, Gottingen, Germany), and statistically analyzed using Image-J software (Version 1.49, National Institutes of Health, Bethesda, USA).

RNA extraction and Quantitative real-time polymerase chain reaction (qRT-PCR)

To examine the gene expression of high glucose-induced HUVECs and HSFs after MSC-CM treatment, RNA extraction and qRT-PCR analysis were performed in our study. Firstly, HUVECs and HSFs were harvested from their control, HG and MSC-CM groups in cellular experimentation and their total RNAs were then extracted with Trizol reagent. After quantified by NanoDrop 2000 (Thermo Fisher Scientific, Inc., MA, USA), total RNAs were reversely transcribed to complementary DNAs which served as a template for qRT-PCR. Secondly, qRT-PCR was carried out in Applied Biosystems StepOnePlus Real-Time PCR System (Thermo Fisher Scientific, Inc., MA, USA) with a running condition as follow: a holding stage (one cycle of 30 sec at 95 °C), a cycling stage (40 cycles of 5 sec at 95 °C and 40 cycles of 30 sec at 60 °C), and a melting curve stage (one cycle of 15 sec at 95 °C, one cycle of 30 sec at 60 °C and one cycle of 15 sec at 95 °C). Finally, the gene expressions of *TNF-α*, *IL-1β*, *IL6*, *ET1*, and *p16* were analyzed in HUVECs and those of *COL1*, *COL3*, *COL4*, *SOD1*, and *SOD2* in HSFs, in which *β-ACTIN* was utilized as a control in the determine of the relative gene expression level. Finally, all data were calculated by the ΔΔCt method and the primer sequences of all genes to be detected were listed in Table 1.

Table 1. Primer sequences used for quantitative real time PCR analysis.

Gene	Forward Primer	Reverse Primer
β-ACTIN	TGGCACCCAGCACAATGAA	CTAAGTCATAGTCCGCCTAGAAGCA
TNF-α	CCTCTCTCTAATCAGCCCTCTG	GAGGACCTGGGAGTAGATGAG
IL-1β	ATGATGGCTTATTACAGTGGCAA	GTCGGAGATTCGTAGCTGGA
IL-6	ACTCACCTCTTCAGAACGAATTG	CCATCTTTGGAAGGTTCAGGTTG
ET1	TAGAGTGTGTCTACTTCTGCCA	TTCTTCCTCTCACTAACTGCTG
p16	CATGGTGCGCAGGTTCTTG	CTTCCAAGTCCATACGGAACAA
COL1	GTGCGATGACGTGATCTGTGA	CGGTGGTTTCTTGGTCGGT
COL3	TGCTGGTCCTGCTGGTCCTAAG	CCAGTAGCACCATCATTTCCACGAG
COL4	GGACTACCTGGAACAAAAGGG	GCCAAGTATCTCACCTGGATCA
SOD1	GATGACTTGGGCAAAGGTGGAAATG	CCAATTACACCACAAGCCAAACGAC
SOD2	CGCCCTGGAACCTCACATCAAC	AACGCCTCCTGGTACTTCTCCTC

Western blot

Western blot (WB) analysis was conducted to determine protein expression of HUVECs and HSFs. After treatment of MSC-CM, HUVECs and HSFs were washed twice with PBS and lysed in RIPA buffer. After centrifuged at 12000 r/min for 10 min at 4 °C, the supernatant of cell lysate was obtained and the protein content was determined by the BCA method according to the manufacturer's instructions of BCA Protein Assay Kit. Then proteins were separated by sodium dodecyl sulfate-polyacrylamide gel electrophoresis (SDS-PAGE) and transferred to polyvinylidene difluoride (PVDF) membranes. Blocked with 5% skimmed milk powder solution at room temperature for 1 h, membranes were then washed four times with Tween in Tris-buffered saline (TTBS) and incubated overnight at 4 °C with primary antibodies including PCNA (HUVECs and HSFs, 1 : 1000 dilution), β-ACTIN (HUVECs and HSFs, 1 : 10000 dilution) and COL1 (HSFs, 1 : 1000 dilution). The membranes were washed four times with TTBS and re-incubated with horseradish peroxidase-conjugated secondary antibodies (1 : 1000 dilution) at room temperature for 1 h. After washing four times with TTBS, the blots in membranes were detected by the ChemiDoc Imaging Systems (Bio-Rad Laboratories, Inc., California, Hercules, USA) and analyzed by Image-J software (Version 1.49, National Institutes of Health, Bethesda, USA).

Statistical analysis

All statistical analyses were performed by SPSS software (Version 26.0, SPSS, Chicago, USA) and OriginPro Software (Version 2021, OriginLab, Northampton, MA, USA). All data were given as mean values ± standard deviation (SD) and comparisons among three or more groups were analyzed by one-way ANOVA followed by least-significant difference (LSD) tests. The results of P-value < 0.05 were considered statistically significant.

Results

Characterization of hucMSCs

For identifying MSCs, the International Society for Cellular Therapy (ISCT) has officially established the following qualifying minimal criteria: low expression (≤ 2%) of negative surface markers (CD34, CD45, and HLA-DR) and high expression (≥ 95%) of positive surface markers (CD105, CD73, and CD90). Among several markers in the results of flow cytometry (Fig. 1), hucMSCs in our cell samples were successfully confirmed due to lowly expressed CD34 (0.18%), CD45 (0.19%), and HLA-DR (0.57%) as well as highly expressed CD73 (99.73%), CD90 (99.96%), and CD105 (99.99%), ensuring the accuracy of subsequent experiments.

hucMSCs-HA gel facilitates foot wound healing of type I diabetic rats

To determine the potential effects of hucMSCs during the diabetic foot wound healing process, an excisional wound model of type I diabetic rat was utilized and the wound healing at different time points was monitored by macroscopic observation. As shown in Fig. 2A, the foot wound surfaces of non-diabetic SD rats in the control group and diabetic SD rats in the MSC-HA group healed as early as 21 days, while the healing time of diabetic SD rats in the T1DM and HA groups exceeded 21 days. Between day 6 and 15, wound surfaces in the control and MSC-HA groups had been gradually reduced with formation of black scabs and alleviation of inflammation, however, those in the T1DM and HA groups were not quickly closed with reduced scabs and inflammation until day 18. By day 21, scabs became detached and new epidermis appeared in the control and MSC-HA groups, while foot wounds in the T1DM and HA groups were not covered with complete epidermis.

Next, the average wound surface healing rates of T1DM rats were measured. As shown in Fig. 2B, the average wound healing rate of diabetic SD rats in the T1DM group had been significantly lower than that in the control group ($P < 0.05$ vs control level) since day 6, which had been improved as a result of HA and MSC-HA treatment ($P < 0.05$ vs T1DM level). On day 6 and 12, the mean wound healing rate of T1DM SD rats was significantly increased in the HA group ($P < 0.05$ vs T1DM level), suggesting that HA was beneficial to slowly promote wound healing of diabetic foot. Along with the beneficial effects of HA, hucMSCs further accelerated the foot wound healing rate in the MSC-HA group from day 6 to 21 ($P < 0.05$ vs T1DM level), demonstrating a similar wound healing trend to normal rats in the control group. Furthermore, between day 6 and 18, the average rate of wound closure in the MSC-HA group was dramatically higher than that in the HA group ($P < 0.05$ vs HA level), suggesting the main therapeutic effects of hucMSCs to diabetic foot.

These results suggested that hucMSC-HA (MSC-HA) gel accelerated the re-epithelialization of diabetic foot in T1DM rats, which mainly benefited from the therapeutic effects of hucMSCs.

hucMSCs-HA gel facilitates foot wound healing of type II diabetic rats

To determine the effects of hucMSCs in promoting the diabetic foot wound healing process, an excisional wound model of type II diabetic rat was also utilized and the wound healing at different time points was monitored by macroscopic observation. As shown in Fig. 3A, wounds in non-diabetic Wistar rats (the control group) could heal with new skin within 18 days, in contrast, complete wound closure time of diabetic GK rats in the T2DM group was over 18 days. After HA and MSC-HA treatment, new crusts of T2DM GK rats grew from the edge of foot wounds and gradually extended to the center during 18 days. Besides, Wistar (the control group) and GK (HA and MSC-HA groups) rats formed scar tissues on day 3, while GK rats in the T2DM group on day 6, and the scars in the four groups were slowly reduced until new epidermis formation between day 3 and 18.

Next, the average wound surface healing rates of T2DM rats were measured. As shown in Fig. 3B, diabetic GK rats in the T2DM group showed a significant reduction in the average foot wound healing rate ($P < 0.05$ vs control level), HA treatment of diabetic foot wounds in the HA group did not show significant effects until 18 days ($P < 0.05$ vs T2DM level), and treatment with MSC-HA had remarkably increased the average foot wound healing rate compared with the T2DM group since day 9 ($P < 0.05$ vs T2DM level) and with the HA group on day 9, 15, and 18 ($P < 0.05$ vs HA level), suggesting an irreplaceable role of hucMSCs in the foot wound contraction process of T2DM GK rats.

These results suggested that hucMSCs-HA (MSC-HA) gel accelerated the re-epithelialization of diabetic foot in T2DM rats, which mainly benefited from the therapeutic effects of hucMSCs.

Histological and immunohistochemical analyses of foot wound healing in type I diabetic rats

To further evaluate the effects of hucMSCs-HA (MSC-HA) gel on diabetic foot wound healing of type I diabetic rats, HE staining, Masson's trichrome staining and immunohistochemistry were performed to analyze the extent of re-epithelialization, collagen deposition and formation of blood vessels, respectively.

As shown in Fig. 4A, HE staining results indicated that wounds of non-diabetic SD rats in the control group completely healed with the new straight epidermis and dermis contained dense connective tissue structures, in contrast, wounds of diabetic SD rats in the T1DM group were not fully re-epithelialized and had severe infiltration of mononuclear leukocytes. In the HA group, the epidermis at the wound of T1DM SD rat was uneven and depressed with the residual scar tissue, and normal thickness was not observed in the dermis with the infiltration of mononuclear leukocytes and polymorphic nuclear leukocytes. Similar to the control group, complete re-epithelialization and dense connective tissue formation were achieved in the MSC-HA group. Moreover, treatment with MSC-HA therapy improved the infiltration of mononuclear leukocytes and polymorphic nuclear leukocytes compared with the T1DM and HA groups.

In Fig. 4B, a large amount of collagen deposition occurred in aligned and wavy fibers of the non-diabetic SD rats (the control group), but relatively less was found in T1DM SD rats (the T1DM group). In both HA and MSC-HA groups, HA and MSC-HA improved collagen synthesis in the wound area of T1DM SD rats. In Fig. 4C, quantitative analysis also revealed that collagen deposition contents in the T1DM group were

significantly lower than those in the control group ($P < 0.01$ vs control level), while HA and MSC-HA treatments significantly increased the collagen deposition ($P < 0.01$ vs T1DM level). Compared with the HA group, a significant increase in collagen deposition was observed in the MSC-HA group ($P < 0.01$ vs HA level), indicating the beneficial effects of hucMSCs grafting in promoting fibrogenic potential in diabetic foot wounds.

In Fig. 4D, 4E and 4F, immunohistochemical analysis indicated that VEGFA positive staining density was detected in the control, T1DM, HA and MSC-HA groups. Among them, both the expression of VEGFA and the number of blood vessels were significantly decreased in the T1DM group ($P < 0.01$ vs control level), which was obviously improved by HA and MSC-HA treatment ($P < 0.01$ vs T1DM level). Compared to HA, hucMSCs further enhanced VEGFA secretion and angiogenesis, as determined by the significantly increased expression of VEGFA protein ($P < 0.05$ vs HA level) and the number of blood vessels ($P < 0.01$ vs HA level) in the MSC-HA group.

These findings demonstrated that both HA gel and hucMSCs-HA gel were beneficial to accelerate re-epithelialization, collagen deposition, and angiogenesis, thus contributing to the foot wound healing of T1DM SD rats, especially hucMSCs-HA gel, in which hucMSCs played an important role.

Histological and immunohistochemical analyses of foot wound healing in type II diabetic rats

To further evaluate the effects of hucMSC-HA (MSC-HA) gel on diabetic foot wound healing of type II diabetic rats, HE staining, Masson's trichrome staining and immunohistochemistry were performed to analyze the extent of re-epithelialization, collagen deposition and angiogenesis, respectively.

In Fig. 5A, HE staining results showed that foot wounds of non-diabetic Wistar rats in the control group were contracted with new and intact skin, whereas those of GK rats in the T2DM group were imperfectly recovered and accompanied by residual scabs, loose vacuolar connective tissue structures, and lots of mononuclear leukocytes and polymorphic nuclear leukocytes. In the HA group (Fig. 5A), the wounds of T2DM GK rats were covered with the non-straight, depressed and papillary epidermis, and had reduced inflammatory cell infiltration. MSC-HA treatment made foot wounds form a flat epidermis without obvious scabs and dense connective tissue similar to the normal group, and further alleviated inflammation compared with the T2DM and HA groups (Fig. 5A). In Fig. 5B and 5C, collagen fibers were synthesized in the control, T2DM, HA and MSC-HA groups. Among them, collagen deposition in the T2DM group was the lowest and the difference against the control group was statistically significant ($P < 0.01$ vs control level). Notably, both HA and MSC-HA groups showed significantly augmented collagen deposition compared with the T2DM group ($P < 0.01$ vs T2DM level), and the MSC-HA group deposited significantly more collagen than the HA group ($P < 0.01$ vs HA level).

As shown in Fig. 5D, 5E and 5F, immunohistochemical results showed that the VEGFA positive staining density and the number of blood vessels of foot wounds in the T2DM group were significantly lower than those in the control group ($P < 0.01$ vs control level). After HA and MSC-HA were implanted in diabetic foot wounds for 19 days, significant increases of the VEGFA expression and the number of blood vessels

were observed, indicating accelerated angiogenesis in the HA and MSC-HA groups ($P < 0.05$ vs T2DM level). Additionally, it was found that hucMSCs further increased the number of blood vessels in the MSC-HA group compared with the HA group ($P < 0.01$ vs HA level).

These results indicated that both HA gel and hucMSCs-HA gel could facilitate foot wounds repair in the T2DM rats through promoting re-epithelialization, collagen deposition and angiogenesis, and hucMSCs-HA gel out-performed HA gel in repairing foot wounds of T2DM rats due to the therapeutic potential of hucMSCs.

The paracrine effects of hucMSCs on the viability and migration of HUVECs and HSFs

To investigate the paracrine effects of hucMSCs on the cell viability and migration of HUVECs and HSFs, MSC-CM was applied in the HG-treated HUVECs and HSFs, and MTT assay, wound healing assay and transwell assay were performed, respectively. As shown in Fig. 6A and 6B, the results of MTT assay showed that the OD values of HUVECs and HSFs in the HG group were significantly lower than those in the control group ($P < 0.01$ vs control level), indicating that HG severely impaired the cell viability of HUVECs and HSFs. After MSC-CM treatment, the cell viability of HUVECs and HSFs was promoted with the significantly increased OD values in the MSC-CM group ($P < 0.01$ vs model level). In wound healing assay, horizontal migrations of HUVECs and HSFs were inhibited under the HG condition, leading to prolonged wound healing with the significantly reduced wound closure rates ($P < 0.01$ vs control level), and such inhibitions of horizontal migrations were improved in the MSC-CM group with the significant increased wound closure rates of HUVECs and HSFs ($P < 0.01$ vs model level) (Fig. 6C, 6D, 6E and 6F). Furthermore, the results of transwell assay showed that the vertical migration of HG-treated HUVECs was obviously slower compared with the control group ($P < 0.01$ vs control level) and treatment of MSC-CM significantly promoted the vertical migration of HUVECs ($P < 0.01$ vs model level) (Fig. 6G and 6H). These results demonstrated that MSC-CM could effectively enhance the cell viability and migration of HG-injured HUVECs and HSFs, suggesting a paracrine-based action mode of hucMSCs.

The paracrine effects of hucMSCs on oxidative stress of HSFs, tubule formation and cell senescence of HUVECs

To investigate the paracrine effects of hucMSCs on oxidative stress of HSFs, tubule formation and senescence of HUVECs, the measurement of MDA and ROS, tube formation assay and SA-β-galactosidase staining were performed, respectively. As shown in Fig. 7A, the MDA level of HSFs was markedly increased in the HG group in comparison to the control group ($P < 0.05$ vs control level), and was significantly reduced after MSC-CM treatment ($P < 0.05$ vs model level). Compared with the control group, the presence of HG significantly enhanced the ROS fluorescent intensity of HSFs, resulting in the ROS accumulation of HSFs ($P < 0.01$ vs control level) (Fig. 7B and 7C). In the MSC-CM group, the remarkable downregulation of ROS levels was observed after MSC-CM treatment for 48 h ($P < 0.01$ vs model level). In Fig. 7F, HUVECs in the control group formed complete tube networks, in contrast, the HG treatment severely disrupted the tube formation of HUVECs, and the statistical analysis of the tube networks showed that number of nodes (Fig. 7D), number of junctions (Fig. 7E), and total tubule length

(Fig. 7G) in the model group were all significantly decreased in the HG group ($P < 0.01$ vs control level). After MSC-CM treatment, the tube network formation of HUVECs was restored and the aforementioned values (number of nodes, number of junctions and total tubule length) were significantly increased ($P < 0.05$ vs model level). Moreover, the SA-β-galactosidase staining results revealed that the percentage of senescent cells in the HG group was obviously higher than that in the control group (Fig. 7H, $P < 0.01$ vs control level), which was dramatically decreased and restored to the normal level by MSC-CM (Fig. 7I, $P < 0.01$ vs model level). Taken together, these results confirmed that MSC-CM could effectively promote tubule formation of HUVECs, and inhibit oxidative stress of HSFs and cell senescence of HUVECs under HG environment.

The paracrine effects of hucMSCs on gene and protein expression of HUVECs and HSFs

To investigate the regulative effects of MSC-CM on gene and protein expressions of HUVECs and HSFs, qRT-PCR and western blot were performed in this study. The results of qRT-PCR indicated that high glucose significantly up-regulated the transcriptional expression levels of pro-inflammatory genes (*TNF-α*, *IL-1β* and *IL-6*), endogenous vasoconstrictor gene (*ET-1*) and senescence gene (*p16*) in HUVECs ($P < 0.05$ or $P < 0.01$ vs control level), and these gene expression levels were remarkably reduced after MSC-CM treatment ($P < 0.05$ or $P < 0.01$ vs model level) (Fig. 8A). Similarly, collagen synthesis (*COL1*, *COL3* and *COL4*) and antioxidant (*SOD1* and *SOD2*) gene expressions of HSFs were significantly down-regulated in the model group ($P < 0.05$ or $P < 0.01$ vs control level), while these gene expression levels were dramatically increased by MSC-CM ($P < 0.05$ or $P < 0.01$ vs control level) (Fig. 8B). Additionally, PCNA expressions were impeded in both HUVECs and HSFs from the HG group ($P < 0.05$ or $P < 0.01$ vs control level), which contrasted with the significant increase of PCNA observed in the both cells treated with MSC-CM ($P < 0.05$ or $P < 0.01$ vs model level) (Fig. 8C and 8D). Also, COL1 expression in the HG group was obviously inhibited compared with the control group ($P < 0.05$ or $P < 0.01$ vs control level), differentially, COL1 in the MSC-CM group was significantly increased ($P < 0.05$ or $P < 0.01$ vs model level).

Discussion

The wound healing is a complex process and treatment difficulty of DFU, for which MSCs therapy has great potential due to its pro-regenerative improvement in tissue cells (e.g., endotheliocytes and fibroblasts). Current studies indicated that MSCs could enhance the proliferation and migration of damaged endotheliocytes and fibroblasts [25, 30] and promote collagen secretion of fibroblasts and tube formation of endotheliocytes [31]. Nowadays, the delivery route options of MSCs for DFU treatment mainly include systemic and topical administrations [32]. Although systemic administration can effectively facilitate cell delivery, most MSCs are easily filtered out in lungs and rarely engraft in distal wound tissues, leading to insufficient repair [33, 34]. Topical administration may be an easier way for DFU treatment, as it avoids the need for long-distance migration of MSCs and reduces the cell loss in lungs and other organs, thus allowing more MSCs to participate in DFU repair [34]. Local injection is the reported topical administration of MSCs, which delivers cells to injury sites through vascular routes [7]. However, the vascular delivery would not be adequately efficient, due to the ‘island’-like deposition of

wound cells, local wound ischemia and hypoxia, imprecisely controlled injection range, and unevenly distributed cells [27, 35]. Herein, this study tried external administration by directly covering MSCs-gel mixture (hucMSCs-HA gel) on the injury sites and obtained satisfactory results. HA gel was used as the carrier of hucMSCs, since it has advantages of inexpensive, good biocompatibility, FDA approved clinical use, and commercially available [36, 37]. This is the first report on the external use of hucMSCs-HA gel for DFU treatment.

This study established DFU models on both type I and type II diabetic rats to evaluate the repairing effects of hucMSCs-HA gel. When compared with the blank gel in the HA group, the hucMSCs-HA gel in the MSC-HA group obviously reduced hemorrhage and inflammatory response as well as promoted granulation tissue formation, collagen deposition, angiogenesis, and re-epithelialization, indicating hucMSCs-enhanced foot wound healing rate of diabetic rats (Fig. 2 to 5). *In vitro*, hucMSCs significantly recovered the HG-caused abnormalities of HUVECs and HSFs through MSC-CM, as determined by cell viability, wound healing, migration, tube formation, senescence, ROS and MDA level assays (Figs. 6 and 7). MSC-CM significantly restored the HG-caused abnormal expressions of inflammatory genes (*TNF-α*, *IL-1β*, and *IL-6*), vasoconstrictive gene (*ET-1*), senescent gene (*p16*), and proliferative protein (PCNA) of HUVECs, and also significantly restored the abnormal expressions of pro-fibrotic genes (*COL1*, *COL3*, *COL4*), antioxidant genes (*SOD1* and *SOD2*), proliferative protein (PCNA), and pro-fibrotic protein (COL1) of HSFs (Fig. 8). Previous studies showed that HA was a useful loading gel for MSCs in treatment of diabetic foot ulcers. For instance, topical injection of hucMSCs with HA accelerated wound healing rate of refractory diabetic foot ulcers in patients [38], and human adipose-derived stem cells (hADSCs)-containing HA enhanced diabetic wound healing by positively impacting re-epithelialization and by modulating the inflammatory response to promote a successful neoinnervation [39]. Comparatively, this study firstly demonstrated dramatic wound healing efficacy of external application of hucMSCs-HA gel on DFU and discovered its paracrine mechanism of action in regard to the improvement of angiogenesis, collagen deposition, and dermal regeneration. Furthermore, the paracrine effects of hucMSCs also involved anti-senescence of HUVECs and anti-oxidative stress of HSFs. The external use of hucMSCs-HA gel might have advantages of longer-term and more direct paracrine effects due to the longer time survival of hucMSCs in HA gel as well as the direct delivery of paracrine factors of huc-MSCs on the wound site. Moreover, direct cover of hucMSCs-HA provided a moist environment, avoided injection injury, and prevented exposure infections, which benefited wound repair and regeneration [27]. In terms of wound healing time and convenient administration, the external use of hucMSCs-HA gel resulted in a better efficacy than other MSCs injection treatment, since the wound closure time in this study was > 3 days shorter than that of other reports using MSCs injection [40]. The innovative highlights of this study were as follows: 1) first evaluation of wound-healing efficacy of hucMSCs-HA gel on DFU by establishing both type I and type II diabetic rat models; 2) first report on external use of hucMSCs-HA gel in treating DFU; 3) determination of paracrine action mode of hucMSCs on HUVECs and HSFs in treatment of DFU.

The actions of MSCs in wound healing contain two main ways: indirect paracrine and direct replacement [41]. The paracrine of MSCs refers to the release of various secretions (growth factors, chemokines, immune factors, and exosomes, etc.), while direct replacement is the differentiation of MSCs into tissue

cells to repair the wound site [42]. These two actions might coexist and function together, but more evidences suggested that the paracrine would be the major way because MSCs hardly survived longer in the recipient tissues [42, 43]. Also, this study confirmed the paracrine effects of hucMSCs on HUVECs and HSFs under HG condition. To discuss the possible paracrine mechanism of hucMSCs, the paracrine molecules and targeting signaling pathways that might participate in the effects of hucMSCs were listed (Table 2). For example, the secretions of MSCs (VEGF, TGF-β1, EGF, miR-146a, and LncRNA H19 etc.) could recruit endotheliocytes and fibroblasts to rapidly proliferate and migrate to wound site of DFU by activating PI3K/Akt pathway, enhancing angiogenesis and promoting collagen synthesis. Further studies are needed for clarification of the paracrine mechanism of hucMSCs-HA gel.

Table 2
Molecular mechanisms of MSCs in treating endotheliocytes and fibroblasts by paracrine action

Paracrine componentss	Target cell	Signaling pathway	Changes in gene expression.	Outcomes	Ref.
miR-17-5p	endotheliocytes	PTEN/AKT/HIF-1α/VEGF pathway ↑	PTEN ↓, p-AKT ↑, HIF-1α ↑, VEGF ↑	proliferation ↑, migration ↑, tube formation ↑, enescence ↓	[44]
IL1ra, IL10, IL13, TGF-β1, BDNF, GDNF, CNTF, HGF, FGF, EGF, VEGF,	endotheliocytes	JAK-STAT pathway ↑, PI3K-Akt pathway ↑, MAPK pathway ↑	TNF-α ↓, IL-1β↓, Selectin-E ↓, p65 ↓, p38 ↓	Inflammation ↓	[45]
VEGF	endotheliocytes	VEGF/VEGFR2 pathway ↑	VEGFR2 ↑	proliferation ↑, apoptosis ↓, inflammation ↓, tube formation ↑	[46]
SDF-1, MCP-1, TGF-β, PDGF-BB, VEGF, VCAM-1, MCP-1	endotheliocytes	SDF-1/CXCR4 axis ↑, MCP-1/CCR2 axis ↑	SDF-1↑, CXCR4 ↑, MCP-1 ↑, CCR2 ↑	proliferation ↑, migration ↑, tube formation ↑	[47]
exosomes-carried miR-135b-5p and miR-499a-3p	endotheliocytes	miR-135b-5p/miR-499a-3p-MEF2C axis ↓	MEF2C ↓	proliferation ↑ migration ↑, tube formation ↑	[48]
VEGF-A, bFGF, Ang-1, aFGF, PDGF	endotheliocytes	integrin β1/ ERK1/2/HIF-1α/ VEGF-A pathway ↑	p-integrin β1 ↑, ERK1/2 ↑, HIF-1α↑, VEGF-A ↑	proliferation ↑ migration ↑, tube formation ↑, senescence ↓	[49]
microvesicles	endotheliocytes	AKT pathway ↑ ERK pathway ↑	cyclin D2 ↑, cyclin A1 ↑, c-Myc ↑, VEGFA ↑, VEGFR2 ↑, FGF2 ↑, HIF-1A ↑, PDGFA ↑, Cox-2 ↑, ITGB1 ↑, CXCL16 ↑, cyclin D1 ↑, cyclin A2 ↑, PDGFR ↑	proliferation ↑, migration ↑, tube formation ↑	[50]

Paracrine componentss	Target cell	Signaling pathway	Changes in gene expression.	Outcomes	Ref.
extracellular vesicles	endotheliocytes	PI3K/AKT/mTOR/HIF-1α pathway ↑	PI3K ↑, AKT ↑, mTOR ↑, p-AKT ↑, p-mTOR ↑, HIF-1α ↑, VEGF ↑	proliferation ↑ migration ↑, tube formation ↑	[51]
exosomes-carried miR-126	endotheliocytes	PI3K/AKT pathway ↑	PTEN ↓, p-AKT ↑	proliferation ↑ migration ↑, tube formation ↑	[52]
extracellular vesicles-carried miR-27b	fibroblasts	ITCH/JUNB/IRE1α pathway ↑	ITCH ↓, JUNB ↑, IRE1α ↑	proliferation ↑ migration ↑	[53]
extracellular vesicles-carried miR-129	endotheliocytes	PTEN/PI3K/AKT pathway ↑	TRAF6 ↓, PTEN ↓,	proliferation ↑ migration ↑, tube formation ↑	[52]
exosomes-carried HMGB1	endotheliocytes	HMGB1/HIF-1α/VEGF pathway ↑, JNK pathway ↑	p-JNK ↑, HIF-1α ↑, VEGF ↑	proliferation ↑ migration ↑, tube formation ↑	[54]
FGF2, VEGFA, TGF-β	endotheliocytes		PLGF ↑, SCF ↑ , VEGFR2 ↑	proliferation ↑ migration ↑, tube formation ↑	[55]
LncRNA H19	endotheliocytes	PTEN/AKT/eNOS pathway ↑	miR-211-3p ↑, PTEN ↓, p-AKT ↑, p-eNOS ↑, PDGF ↑, EGF ↑, bFGF ↑, VEGF ↑, ANG1 ↑	proliferation ↑ migration ↑, tube formation ↑, invasion ↑	[56]
lncRNA H19	endotheliocytes	lncRNA H19/miR-152-3p/PTEN axis ↑ PTEN/PI3K/AKT pathway ↓	PTEN ↑, miR-152-3p ↑, p85 PI3K ↓, AKT ↓	proliferation ↑, migration ↑, apoptosis ↓, inflammation ↓	[57]
miR-146a	endotheliocytes	miR-146a/Src axis ↓	p-Src ↓, p-VE-cadherin ↓, p-Caveolin-1 ↓, SASP ↓, p16, ↓ p21 ↓, p53 ↓	proliferation ↑ migration ↑, tube formation ↑, senescence ↓	[58]

Paracrine componentss	Target cell	Signaling pathway	Changes in gene expression.	Outcomes	Ref.
exosomes	endotheliocytes		NOX1↓, NOX4 ↓, cyclin D1 ↓, cyclin D3 ↓, IL-1β ↓, IL-6 ↓, TNF-α ↓	proliferation ↑, angiogenesis ↑, oxidative stress ↓, inflammation ↓	[59]
exosomes	endotheliocytes	PI3K/AKT/eNOS pathway ↑	PTEN ↓, p-AKT ↑, p-PI3K ↑, p-eNOS ↑, Cyclin D1 ↑, Cyclin D3 ↑, VEGF↑	proliferation ↑ migration ↑, tube formation ↑ invasion ↑, nitric oxide ↑	[60]
IL-6; VEGF, MCP-1, angiogenin	endotheliocytes	PI3K/Akt pathway ↑	p-Akt ↑, p-ERK ↑	proliferation ↑, migration ↑, tube formation ↑, invasion ↑	[25]
IL-8, IL-6, TGF-β , TNFRI, VEGF, EGF	fibroblasts	TGF-β/SMAD2 pathway ↑	p-SMAD2 ↑	proliferation ↑, migration ↑	[61]
Wnt4, G-CSF, PDGF-BB, VEGF, MCP-1, IL-6, IL-8	fibroblasts	Wnt4/β-catenin pathway ↑ AKT pathway ↑	β-catenin ↑, CK19 ↑, PCNA ↑, collagen I ↑	proliferation ↑, migration ↑	[62]
exosomes	fibroblasts	ERK/MAPK pathway ↑	MMP3 ↑, TIMP1 ↑	proliferation ↑, migration ↑	[63]
exosomes	fibroblasts	PI3K/Akt pathway ↑	bFGF ↑, TGF-β1 ↑, collagen I ↑, collagen III ↑,	collagen synthesis ↑	[64]
TGF-β1, IL-6, IL-8, MCP-1, RANTES, HGF, SPARC, IGFBP-7	fibroblasts	HGF/c-met axis ↑	HGF ↑, c-met ↑	migration ↑	[47]

Paracrine componentss	Target cell	Signaling pathway	Changes in gene expression.	Outcomes	Ref.
bFGF, IGF-1, VEGFA, TGFβ-2, TGFβ-3, IL-1β, IL-6, IL-8	fibroblasts	TGF-β/SMAD pathway ↑	p-SMAD2/3 ↑, SMAD7 ↑, p21, p16	oxidative stress ↓ ROS overproduction ↓ senescence ↓ myofibroblast formation ↓	[65]
EGF, bFGF, TGF-b, PDGF, HGF, EGF, pro-collagen I	fibroblasts		collagen I ↑, collagen III ↑, fibronectin ↑, flastin ↑	proliferation ↑, migration ↑	[66]
VEGF, FGF2, TGF-β1, IL6	fibroblasts	TGF-β/SMAD2 pathway ↑, PI3K/AKT pathway ↑	Fibronectin ↑, p-AKT ↑, p-SMAD2 ↑	proliferation ↑ migration ↑ collagen synthesis ↑	[65]

Conclusion

This study firstly reported that external use of hucMSCs-HA gel exerted a therapeutic potential in treating DFU, as evidenced by its beneficial wound-healing efficacy in both type I and type II diabetic rat models as well as paracrine effects on HUVECs and HSFs. The *in vivo* data demonstrated that hucMSCs-HA gel promoted re-epithelialization, collagen deposition, and angiogenesis of DFU wound sites in both type I and type II diabetic rats, in which HA served as drug carrier and hucMSCs played a paracrine role. The *in vitro* data further confirmed the paracrine beneficial effects of hucMSCs on HUVECs and HSFs by restoring high glucose-caused abnormalities of cell viability, migration, oxidative stress, angiogenesis, and cell senescence. Regrettably, chemical, physical, and biological properties (solubility, degradability, swelling, and antibacterial activity, etc.) of hucMSCs-HA gel were not analyzed and molecular mechanisms of hucMSCs in treating DFU by paracrine action were not determined, which provided the direction of our further research. Collectively, our findings provided novel knowledge of hucMSCs-HA gel in the topical treatment of DFU and suggested a prospective strategy for the clinical treatment of DFU.

Abbreviations

MSCs: mesenchymal stem cells

hucMSCs: human umbilical cord-derived mesenchymal stem cells

HA: hyaluronic acid

HUVECs: human umbilical vein endothelial cells

HSFs: human skin fibroblasts

MSC-CM: conditioned medium of hucMSCs

ROS: reactive oxygen species

ET-1: endothelin-1

IL-6: interleukin-6

TNF-α: tumor necrosis factor-alpha

COL1: collagen I

COL3: collagen III

COL4: collagen IV

PCNA: proliferating cell nuclear antigen

STZ: streptozotocin

Declarations

Ethics approval and consent to participate

Great care was taken to minimize their suffering and this study was approved by the Animal Ethics Committee of Zhejiang Chinese Medical University (Animal Ethics No: 11410).

Consent for publication

Not applicable.

Availability of data and materials

The data that support the findings of this study are available from the corresponding author upon reasonable request.

Competing interests

The authors have declared that no competing interest exists.

Funding

This work was supported by National Natural Science Foundation of China (Grant No.81973767), Hangzhou Science and Technology Development Program (Grant No. 20180533B38), Zhejiang University Student Science and Technology Innovation Activity Plan and New Seed Talent Project (Grant No. 2021R410059).

Authors' contributions

Jingan Chen conducted the main work of this study; Jingan Chen, Yi Liu and Haowei Liang conducted to the animal experiment; Li Yan contributed to the hucMSCs preparation and quality control; Yi Liu, Ting Li, Jingwen Zhang contributed to the cellular and molecular experiments; Li Zhou provided ideas and designed this study; Jingan Chen contributed drafted this manuscript; Li Zhou, Letian Shan and Hui Wang designed, drafted, and funded this study. All authors have read and approved the manuscript.

Acknowledgements

Not applicable

Author information

[1]College of Pharmaceutical Sciences, Zhejiang Chinese Medical University, Hangzhou, China. [2]The First Affiliated Hospital, Zhejiang Chinese Medical University, Hangzhou, China. [3]Cell Resource Bank and Integrated Cell Preparation Center of Xiaoshan District, Hangzhou Regional Cell preparation center (Shangyu Biotechnology Co., Ltd), Hangzhou, China.

References

1. Sun H, Saeedi P, Karuranga S, Pinkepank M, Ogurtsova K, Duncan BB, Stein C, Basit A, Chan JCN, Mbanya JC, et al. IDF Diabetes Atlas: Global, regional and country-level diabetes prevalence estimates for 2021 and projections for 2045. Diabetes Res Clin Pract. 2022;183:109119.
2. Aronson R, Chu L, Joseph N, Brown R. Prevalence and Risk Evaluation of Diabetic Complications of the Foot Among Adults With Type 1 and Type 2 Diabetes in a Large Canadian Population (PEDAL Study). Can J Diabetes. 2021;45(7):588–93.
3. Røikjer J, Werkman NCC, Ejskjaer N, van den Bergh JPW, Vestergaard P, Schaper NC, Jensen MH, Klungel O, de Vries F, Nielen JTH, et al: Incidence, hospitalization and mortality and their changes over time in people with a first ever diabetic foot ulcer. Diabetic Medicine 2021:e14725.
4. Apelqvist J, Bakker K, van Houtum WH, Nabuurs-Franssen MH, Schaper NC. International consensus and practical guidelines on the management and the prevention of the diabetic foot. International Working Group on the Diabetic Foot. Diab/Metab Res Rev 2000, 16 Suppl 1:84–92.
5. Hangaard S, Rasmussen A, Almdal T, Nielsen AA, Nielsen KE, Siersma V, Holstein P. Standard complication screening information can be used for risk assessment for first time foot ulcer among patients with type 1 and type 2 diabetes. Diabetes Res Clin Pract. 2019;151:177–86.

6. Cavanagh PR, Lipsky BA, Bradbury AW, Botek G. Treatment for diabetic foot ulcers. Lancet. 2005;366(9498):1725–35.
7. Chastain CA, Klopfenstein N, Serezani CH, Aronoff DM. A Clinical Review of Diabetic Foot Infections. Clin Podiatr Med Surg. 2019;36(3):381–95.
8. Moore ZE, Webster J. Dressings and topical agents for preventing pressure ulcers. Cochrane Database of Systematic Reviews 2013(8):Cd009362.
9. Skórkowska-Telichowska K, Kulma A, Szopa J. The response of diabetic foot to a new type of dressing. Arch Intern Med. 2012;5(1):33.
10. Perez-Favila A, Martinez-Fierro ML, Rodriguez-Lazalde JG, Cid-Baez MA, Zamudio-Osuna MJ, Martinez-Blanco MDR, Mollinedo-Montaño FE, Rodriguez-Sanchez IP, Castañeda-Miranda R, Garza-Veloz I: Current Therapeutic Strategies in Diabetic Foot Ulcers. Medicina (Kaunas, Lithuania) 2019, 55(11).
11. Holl J, Kowalewski C, Zimek Z, Fiedor P, Kaminski A, Oldak T, Moniuszko M, Eljaszewicz A. Chronic Diabetic Wounds and Their Treatment with Skin Substitutes. Cells 2021, 10(3).
12. Tahir AR, Westhuyzen J, Dass J, Collins MK, Webb R, Hewitt S, Fon P, McKay M. Hyperbaric oxygen therapy for chronic radiation-induced tissue injuries: Australasia's largest study. Asia-Pac J Clin Oncol. 2015;11(1):68–77.
13. Anagnostakos K, Thiery A, Sahan I. Retained Negative Pressure Wound Therapy Foams as a Cause of Infection Persistence. Adv wound care. 2021;10(12):699–710.
14. Bardill JR, Laughter MR, Stager M, Liechty KW, Krebs MD, Zgheib C. Topical gel-based biomaterials for the treatment of diabetic foot ulcers. Acta Biomater. 2022;138:73–91.
15. Chen X, Wu J, Cao X, Jiang H, Wu Z, Zeng Z, Chen H, Zhang J. The role of gel wound dressings loaded with stem cells in the treatment of diabetic foot ulcers. Am J translational Res. 2021;13(12):13261–72.
16. Jo H, Brito S, Kwak BM, Park S, Lee MG, Bin BH. Applications of Mesenchymal Stem Cells in Skin Regeneration and Rejuvenation. International journal of molecular sciences 2021, 22(5).
17. Fu X, Liu G, Halim A, Ju Y, Luo Q, Song AG. Mesenchymal Stem Cell Migration and Tissue Repair Cells. 2019;8(8):784–802.
18. Pixley JS. Mesenchymal stem cells to treat type 1 diabetes. Biochim et Biophys acta Mol basis disease. 2020;1866(4):165315.
19. Bhansali S, Dutta P, Kumar V, Yadav MK, Jain A, Mudaliar S, Bhansali S, Sharma RR, Jha V, Marwaha N, et al. Efficacy of Autologous Bone Marrow-Derived Mesenchymal Stem Cell and Mononuclear Cell Transplantation in Type 2 Diabetes Mellitus: A Randomized, Placebo-Controlled Comparative Study. Stem Cells Dev. 2017;26(7):471–81.
20. Zhou Y, Hu Q, Chen F, Zhang J, Guo J, Wang H, Gu J, Ma L, Ho G. Human umbilical cord matrix-derived stem cells exert trophic effects on β-cell survival in diabetic rats and isolated islets. Dis Models Mech. 2015;8(12):1625–33.

21. Maranda EL, Rodriguez-Menocal L, Badiavas EV. Role of Mesenchymal Stem Cells in Dermal Repair in Burns and Diabetic Wounds. Curr Stem Cell Res Therapy. 2017;12(1):61–70.
22. Xiong J, Hu H, Guo R, Wang H, Jiang H. Mesenchymal Stem Cell Exosomes as a New Strategy for the Treatment of Diabetes Complications. Front Endocrinol. 2021;12:646233.
23. Moon KC, Suh HS, Kim KB, Han SK, Young KW, Lee JW, Kim MH. Potential of Allogeneic Adipose-Derived Stem Cell-Hydrogel Complex for Treating Diabetic Foot Ulcers. Diabetes. 2019;68(4):837–46.
24. Casado-Díaz A, Quesada-Gómez JM, Dorado G. Extracellular Vesicles Derived From Mesenchymal Stem Cells (MSC) in Regenerative Medicine: Applications in Skin Wound Healing. Front Bioeng Biotechnol. 2020;8:146.
25. An T, Chen Y, Tu Y, Lin P. Mesenchymal Stromal Cell-Derived Extracellular Vesicles in the Treatment of Diabetic Foot Ulcers: Application and Challenges. Stem cell reviews and reports. 2021;17(2):369–78.
26. Shi R, Lian W, Jin Y, Cao C, Han S, Yang X, Zhao S, Li M, Zhao H. Role and effect of vein-transplanted human umbilical cord mesenchymal stem cells in the repair of diabetic foot ulcers in rats. Acta Biochim Biophys Sin. 2020;52(6):620–30.
27. Zhao Y, Wang M, Liang F, Li J. Recent strategies for enhancing the therapeutic efficacy of stem cells in wound healing. Stem Cell Res Ther. 2021;12(1):588.
28. Guest PC: Characterization of the Goto-Kakizaki (GK) Rat Model of Type 2 Diabetes. Methods in molecular biology (Clifton, NJ) 2019, 1916:203–211.
29. Portha B, Lacraz G, Chavey A, Figeac F, Fradet M, Tourrel-Cuzin C, Homo-Delarche F, Giroix MH, Bailbé D, Gangnerau MN, et al: Islet structure and function in the GK rat. Advances in experimental medicine and biology 2010, 654:479–500.
30. Cao Y, Gang X, Sun C, Wang G. Mesenchymal Stem Cells Improve Healing of Diabetic Foot Ulcer. J Diabetes Res. 2017;2017:9328347.
31. Zhang J, Guan J, Niu X, Hu G, Guo S, Li Q, Xie Z, Zhang C, Wang Y. Exosomes released from human induced pluripotent stem cells-derived MSCs facilitate cutaneous wound healing by promoting collagen synthesis and angiogenesis. J translational Med. 2015;13:49.
32. Yan J, Liang J, Cao Y, El Akkawi MM, Liao X, Chen X, Li C, Li K, Xie G, Liu H. Efficacy of topical and systemic transplantation of mesenchymal stem cells in a rat model of diabetic ischemic wounds. Stem Cell Res Ther. 2021;12(1):220.
33. Kallmeyer K, André-Lévigne D, Baquié M, Krause KH, Pepper MS, Pittet-Cuénod B, Modarressi A. Fate of systemically and locally administered adipose-derived mesenchymal stromal cells and their effect on wound healing. Stem cells translational medicine. 2020;9(1):131–44.
34. Manieri NA, Stappenbeck TS. Mesenchymal stem cell therapy of intestinal disease: are their effects systemic or localized? Curr Opin Gastroenterol. 2011;27(2):119–24.
35. Zhang AJ, Jiang T, Li Q, Jin PS, Tan Q. Experimental research on ADSCs-NCSS in wound repair. Experimental and therapeutic medicine. 2018;16(6):4429–36.

36. Agarwal G, Agiwal S, Srivastava A. Hyaluronic acid containing scaffolds ameliorate stem cell function for tissue repair and regeneration. Int J Biol Macromol. 2020;165(Pt A):388–401.
37. Alemzadeh E, Oryan A, Mohammadi AA. Hyaluronic acid hydrogel loaded by adipose stem cells enhances wound healing by modulating IL-1β, TGF-β1, and bFGF in burn wound model in rat. J biomedical Mater Res Part B Appl biomaterials. 2020;108(2):555–67.
38. Zhao L, Guo Z, Chen K, Yang W, Wan X, Zeng P, He H, Luo Y, Xiao Q, Mo Z. Combined Transplantation of Mesenchymal Stem Cells and Endothelial Colony-Forming Cells Accelerates Refractory Diabetic Foot Ulcer Healing. Stem cells international 2020, 2020:8863649.
39. da Silva LP, Santos TC, Rodrigues DB, Pirraco RP, Cerqueira MT, Reis RL, Correlo VM, Marques AP. Stem Cell-Containing Hyaluronic Acid-Based Spongy Hydrogels for Integrated Diabetic Wound Healing. J Invest Dermatol. 2017;137(7):1541–51.
40. Yan W, Liu H, Deng X, Jin Y, Sun H, Li C, Wang N, Chu J. Raman spectroscopy enables noninvasive biochemical identification of the collagen regeneration in cutaneous wound healing of diabetic mice treated with MSCs. Lasers Med Sci. 2017;32(5):1131–41.
41. D'Souza N, Rossignoli F, Golinelli G, Grisendi G, Spano C, Candini O, Osturu S, Catani F, Paolucci P, Horwitz EM, et al. Mesenchymal stem/stromal cells as a delivery platform in cell and gene therapies. BMC Med. 2015;13:186.
42. Aldrich ED, Cui X, Murphy CA, Lim KS, Hooper GJ, McIlwraith CW, Woodfield TBF. Allogeneic mesenchymal stromal cells for cartilage regeneration: A review of in vitro evaluation, clinical experience, and translational opportunities. Stem cells translational medicine. 2021;10(11):1500–15.
43. Cossu G, Birchall M, Brown T, De Coppi P, Culme-Seymour E, Gibbon S, Hitchcock J, Mason C, Montgomery J, Morris S, et al. Lancet Commission: Stem cells and regenerative medicine. Lancet. 2018;391(10123):883–910.
44. Wei Q, Wang Y, Ma K, Li Q, Li B, Hu W, Fu X, Zhang C. Extracellular Vesicles from Human Umbilical Cord Mesenchymal Stem Cells Facilitate Diabetic Wound Healing Through MiR-17-5p-mediated Enhancement of Angiogenesis. Stem cell reviews and reports. 2022;18(3):1025–40.
45. Zhong L, Yang M, Zou X, Du T, Xu H, Sun J. Human umbilical cord multipotent mesenchymal stromal cells alleviate acute ischemia-reperfusion injury of spermatogenic cells via reducing inflammatory response and oxidative stress. Stem Cell Res Ther. 2020;11(1):294.
46. Yang J, Su J, Xi SS, Ke XF, Zhu Y, Lin HP, Zeng XK, Liu BW, Zhu ML, Dai WY, et al. Human umbilical cord mesenchymal stem cells pretreated with Angiotensin-II attenuate pancreas injury of rats with severe acute pancreatitis. 117: Biomedicine & pharmacotherapy = Biomedecine & pharmacotherapie; 2019. p. 109052.
47. Shen C, Lie P, Miao T, Yu M, Lu Q, Feng T, Li J, Zu T, Liu X, Li H. Conditioned medium from umbilical cord mesenchymal stem cells induces migration and angiogenesis. Mol Med Rep. 2015;12(1):20–30.
48. Yang K, Li D, Wang M, Xu Z, Chen X, Liu Q, Sun W, Li J, Gong Y, Liu D, et al. Exposure to blue light stimulates the proangiogenic capability of exosomes derived from human umbilical cord mesenchymal stem cells. Stem Cell Res Ther. 2019;10(1):358.

49. Wu M, Chen L, Qi Y, Ci H, Mou S, Yang J, Yuan Q, Yao W, Wang Z, Sun J. Human umbilical cord mesenchymal stem cell promotes angiogenesis via integrin β1/ERK1/2/HIF-1α/VEGF-A signaling pathway for off-the-shelf breast tissue engineering. Stem Cell Res Ther 2022, 13(1):99.
50. Ren S, Chen J, Duscher D, Liu Y, Guo G, Kang Y, Xiong H, Zhan P, Wang Y, Wang C, et al. Microvesicles from human adipose stem cells promote wound healing by optimizing cellular functions via AKT and ERK signaling pathways. Stem Cell Res Ther. 2019;10(1):47.
51. Liu W, Yuan Y, Liu D. Extracellular Vesicles from Adipose-Derived Stem Cells Promote Diabetic Wound Healing via the PI3K-AKT-mTOR-HIF-1α Signaling Pathway. Tissue Eng regenerative Med. 2021;18(6):1035–44.
52. Ding J, Wang X, Chen B, Zhang J, Xu J: Exosomes Derived from Human Bone Marrow Mesenchymal Stem Cells Stimulated by Deferoxamine Accelerate Cutaneous Wound Healing by Promoting Angiogenesis. BioMed research international 2019, 2019:9742765.
53. Cheng S, Xi Z, Chen G, Liu K, Ma R, Zhou C. Extracellular vesicle-carried microRNA-27b derived from mesenchymal stem cells accelerates cutaneous wound healing via E3 ubiquitin ligase ITCH. J Cell Mol Med. 2020;24(19):11254–71.
54. Gao W, He R, Ren J, Zhang W, Wang K, Zhu L, Liang T. Exosomal HMGB1 derived from hypoxia-conditioned bone marrow mesenchymal stem cells increases angiogenesis via the JNK/HIF-1α pathway. FEBS open bio. 2021;11(5):1364–73.
55. Jin S, Yang C, Huang J, Liu L, Zhang Y, Li S, Zhang L, Sun Q, Yang P. Conditioned medium derived from FGF-2-modified GMSCs enhances migration and angiogenesis of human umbilical vein endothelial cells. Stem Cell Res Ther. 2020;11(1):68.
56. Yu M, Liu W, Li J, Lu J, Lu H, Jia W, Liu F. Exosomes derived from atorvastatin-pretreated MSC accelerate diabetic wound repair by enhancing angiogenesis via AKT/eNOS pathway. Stem Cell Res Ther. 2020;11(1):350.
57. Li B, Luan S, Chen J, Zhou Y, Wang T, Li Z, Fu Y, Zhai A, Bi C. The MSC-Derived Exosomal lncRNA H19 Promotes Wound Healing in Diabetic Foot Ulcers by Upregulating PTEN via MicroRNA-152-3p. Mol therapy Nucleic acids. 2020;19:814–26.
58. Xiao X, Xu M, Yu H, Wang L, Li X, Rak J, Wang S, Zhao RC. Mesenchymal stem cell-derived small extracellular vesicles mitigate oxidative stress-induced senescence in endothelial cells via regulation of miR-146a/Src. Signal Transduct Target therapy. 2021;6(1):354.
59. Yan C, Xv Y, Lin Z, Endo Y, Xue H, Hu Y, Hu L, Chen L, Cao F, Zhou W, et al. Human Umbilical Cord Mesenchymal Stem Cell-Derived Exosomes Accelerate Diabetic Wound Healing via Ameliorating Oxidative Stress and Promoting Angiogenesis. Front Bioeng Biotechnol. 2022;10:829868.
60. Hu Y, Tao R, Chen L, Xiong Y, Xue H, Hu L, Yan C, Xie X, Lin Z, Panayi AC, et al. Exosomes derived from pioglitazone-pretreated MSCs accelerate diabetic wound healing through enhancing angiogenesis. J Nanobiotechnol. 2021;19(1):150.
61. Yoon BS, Moon JH, Jun EK, Kim J, Maeng I, Kim JS, Lee JH, Baik CS, Kim A, Cho KS, et al. Secretory profiles and wound healing effects of human amniotic fluid-derived mesenchymal stem cells. Stem

Cells Dev. 2010;19(6):887–902.

62. Zhang B, Wang M, Gong A, Zhang X, Wu X, Zhu Y, Shi H, Wu L, Zhu W, Qian H, et al. HucMSC-Exosome Mediated-Wnt4 Signaling Is Required for Cutaneous Wound Healing. Stem Cells. 2015;33(7):2158–68.
63. Wang L, Hu L, Zhou X, Xiong Z, Zhang C, Shehada HMA, Hu B, Song J, Chen L. Exosomes secreted by human adipose mesenchymal stem cells promote scarless cutaneous repair by regulating extracellular matrix remodelling. Sci Rep. 2017;7(1):13321.
64. Zhang W, Bai X, Zhao B, Li Y, Zhang Y, Li Z, Wang X, Luo L, Han F, Zhang J, et al. Cell-free therapy based on adipose tissue stem cell-derived exosomes promotes wound healing via the PI3K/Akt signaling pathway. Exp Cell Res. 2018;370(2):333–42.
65. Jun EK, Zhang Q, Yoon BS, Moon JH, Lee G, Park G, Kang PJ, Lee JH, Kim A, You S. Hypoxic conditioned medium from human amniotic fluid-derived mesenchymal stem cells accelerates skin wound healing through TGF-β/SMAD2 and PI3K/Akt pathways. Int J Mol Sci. 2014;15(1):605–28.
66. Hendrawan S, Kusnadi Y, Lagonda CA, Fauza D, Lheman J, Budi E, Manurung BS, Baer HU, Tansil Tan S. Wound healing potential of human umbilical cord mesenchymal stem cell conditioned medium: An in vitro and in vivo study in diabetes-induced rats. Veterinary world. 2021;14(8):2109–17.

Figures

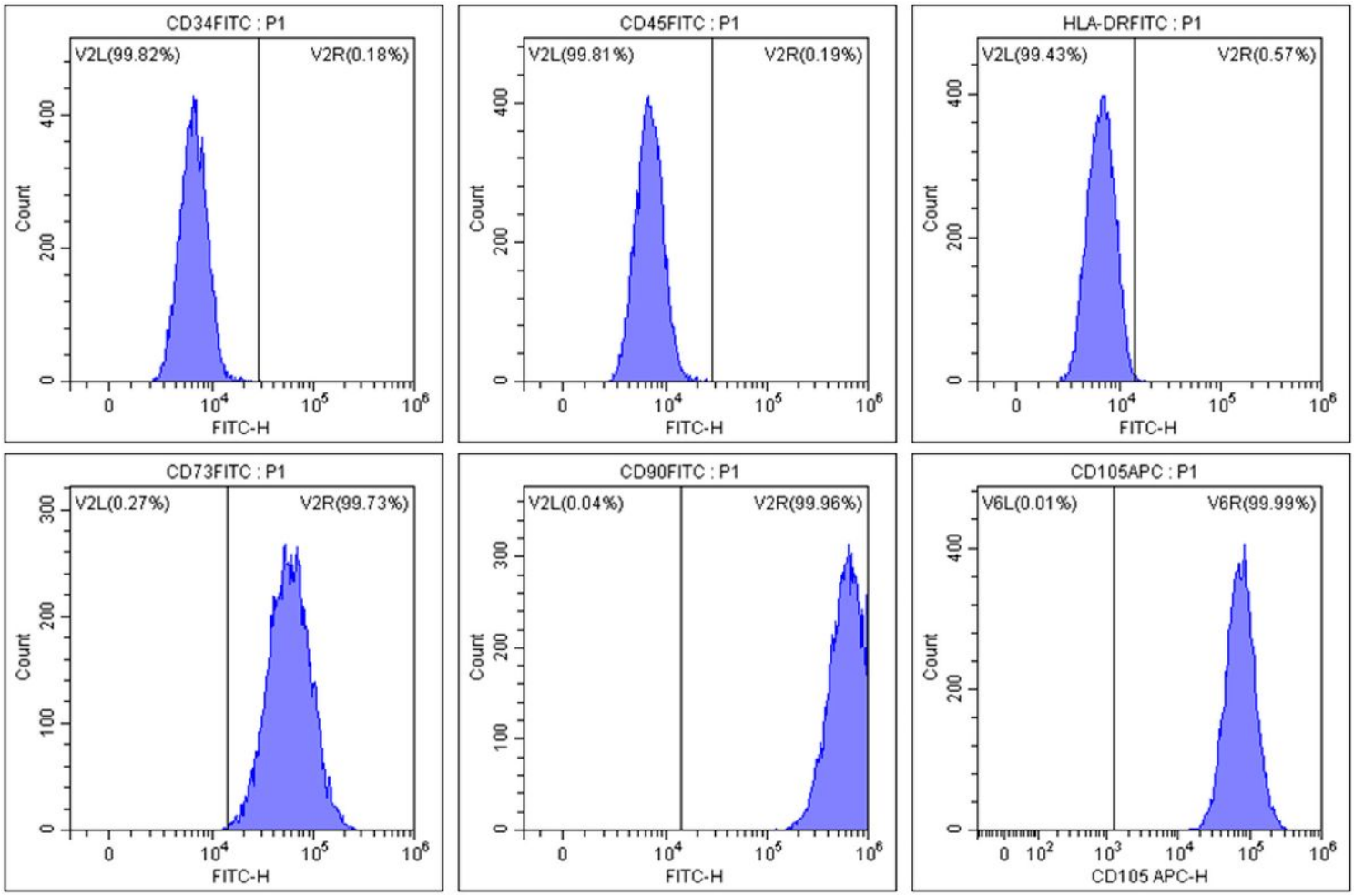

Figure 1

Flow cytometric analysis of hucMSCs surface markers (CD34, CD45, HLA-DR, CD73, CD90, and CD105).

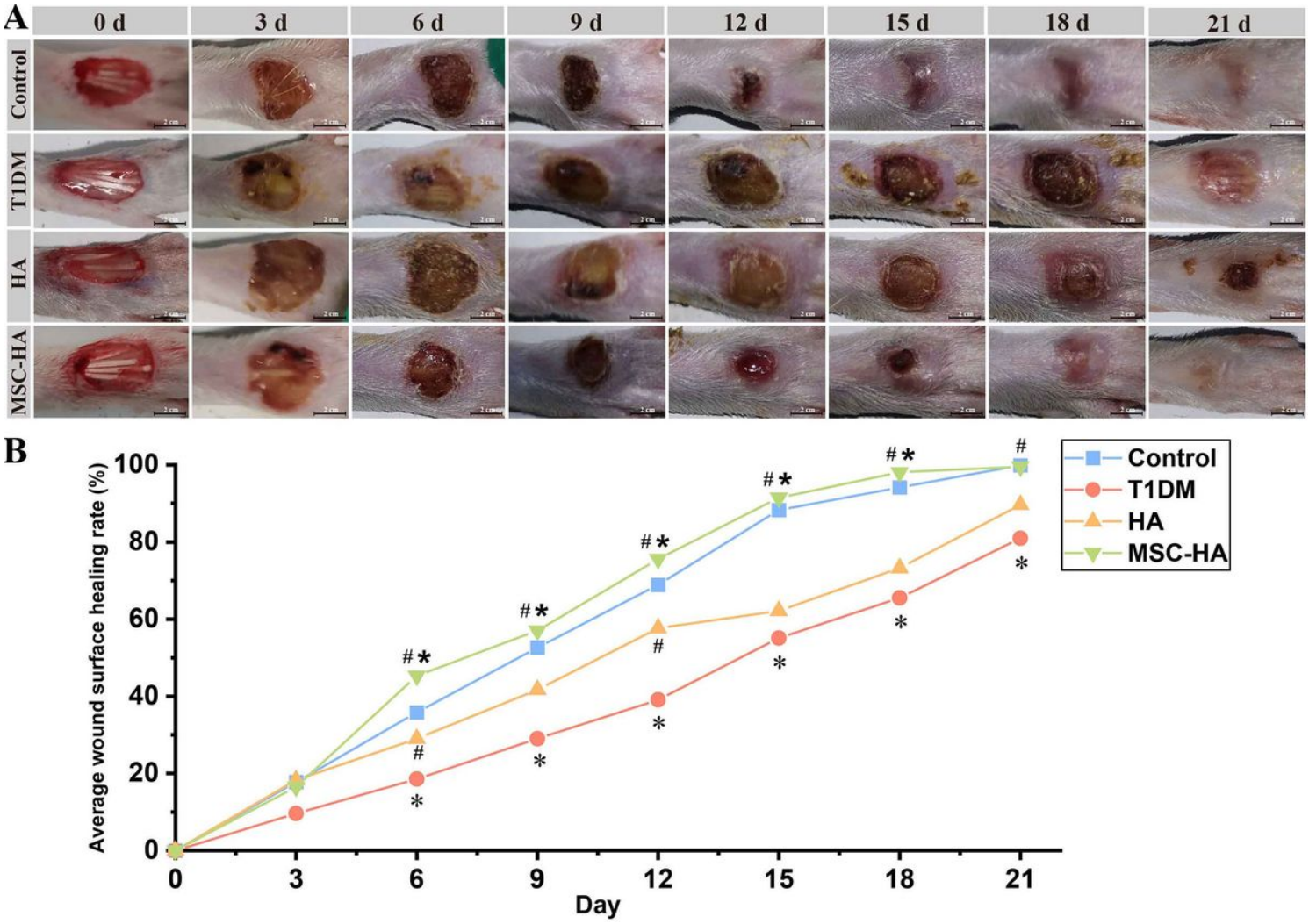

Figure 2

Treatment effects of hucMSCs-HA gel on healing of type I diabetic foot wounds at different time points. (A) Representative digital images of wound healing surfaces in SD rats on day 0, 3, 6, 9, 2, 15, 18, and 21, including the control, T1DM, HA and MSC-HA groups. (B) Line graph of average wound surface healing rate in SD rats. *P < 0.05 and **P < 0.01 vs the control group, $^{\#}P$ < 0.05 and $^{\#\#}P$ < 0.01 vs the model (T1DM) group, *P < 0.05 and **P < 0.01 vs the HA group.

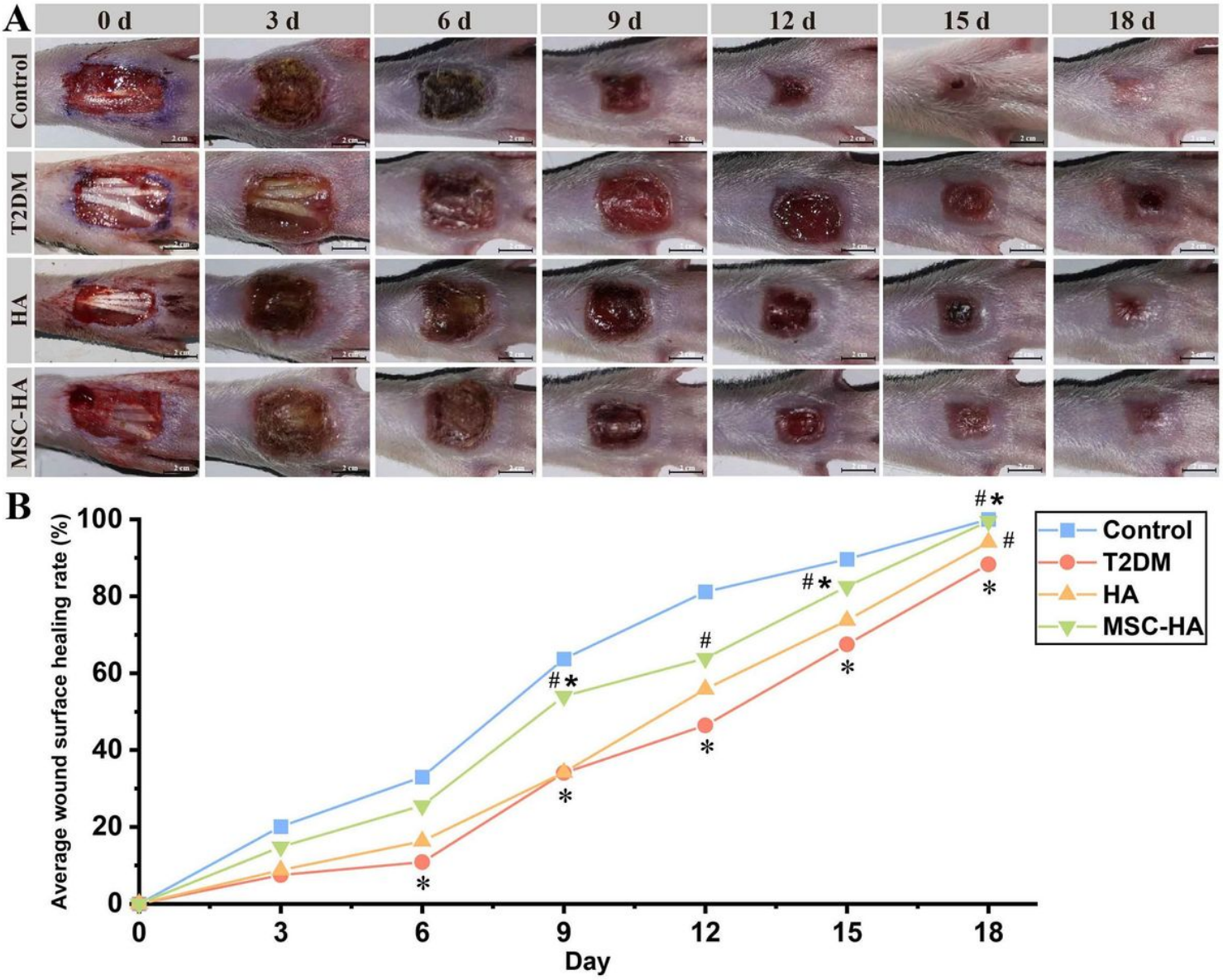

Figure 3

Treatment effects of hucMSCs-HA gel on healing of type II diabetic foot wounds at different time points. (A) Representative digital images of wound healing surfaces in Wistar and GK rats on day 0, 3, 6, 9, 2, 15, and 18, including the control, T2DM, HA and MSC-HA groups. (B) Line graph of wound surface average healing rate in Wistar and GK rats. *P < 0.05 and **P < 0.01 vs the control group, $^{\#}P$ < 0.05 and $^{\#\#}P$ < 0.01 vs the model (T2DM) group, *P < 0.05 and **P < 0.01 vs the HA group.

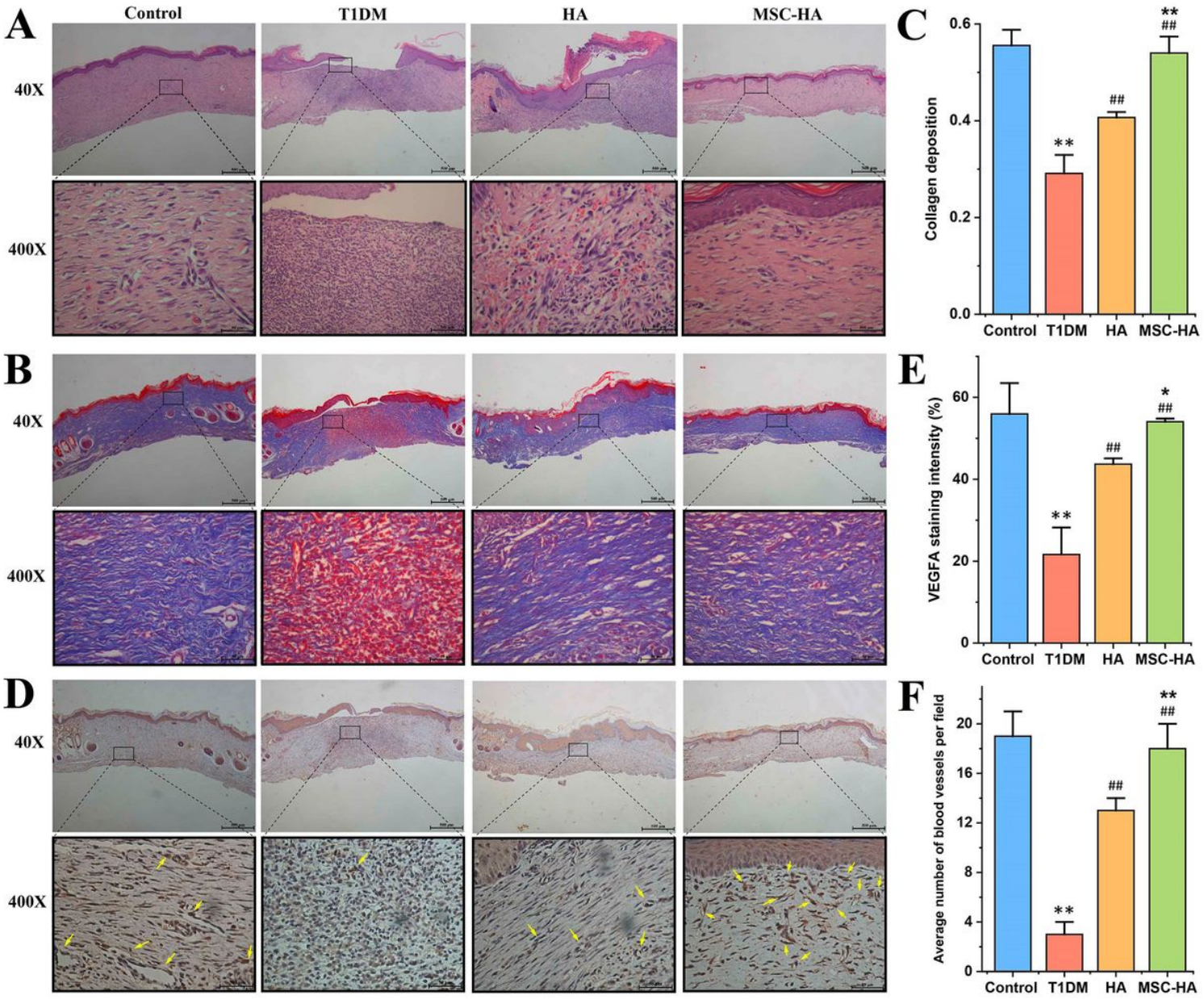

Figure 4

Histopathological features of diabetic foot wounds closure in the control, T1DM, HA, and MSC-HA groups. (A) Representative micrographs of HE staining (40× and 400×). (B) Representative micrographs of Masson's trichrome stained sections (40× and 400×). (C) Histogram of collagen deposition from Masson's trichrome. (D) Representative micrographs of VEGFA antibody immunohistochemistry and blood vessels labeled by yellow allows (40× and 400×). (E) Histogram of immunohistochemical staining intensity (VEGFA antibody). (F) Histogram of average number of blood vessels. Data were mean ± SD. *P < 0.05 and **P < 0.01 vs the control group, $^{\#}P$ < 0.05 and $^{\#\#}P$ < 0.01 vs the model group, *P < 0.05 and **P < 0.01 vs the HA group.

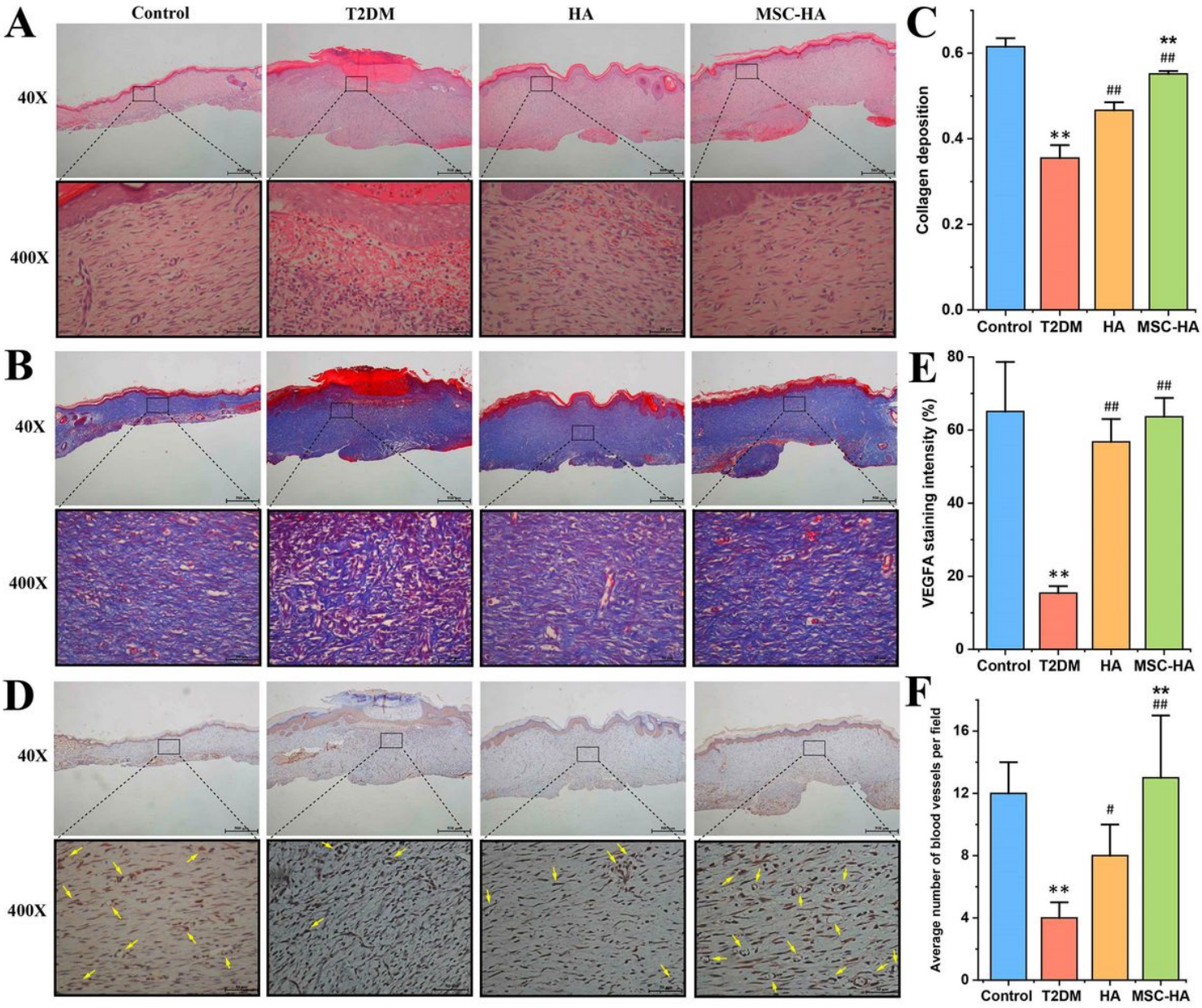

Figure 5

Histopathological features of diabetic foot wounds closure in the control, T2DM, HA, and MSC-HA groups. (A) Representative micrographs of HE staining (40× and 400×). (B) Representative micrographs of Masson's trichrome stained sections (40× and 400×). (C) Histogram of collagen deposition from Masson's trichrome. (D) Representative micrographs of VEGFA antibody immunohistochemistry and blood vessels labeled by yellow allows (40× and 400×). (E) Histogram of immunohistochemical staining intensity (VEGFA antibody). (F) Histogram of average number of blood vessels. Data were mean ± SD. $^{*}P < 0.05$ and $^{**}P < 0.01$ vs the control group, $^{\#}P < 0.05$ and $^{\#\#}P < 0.01$ vs the model group, $^{*}P < 0.05$ and $^{**}P < 0.01$ vs the HA group.

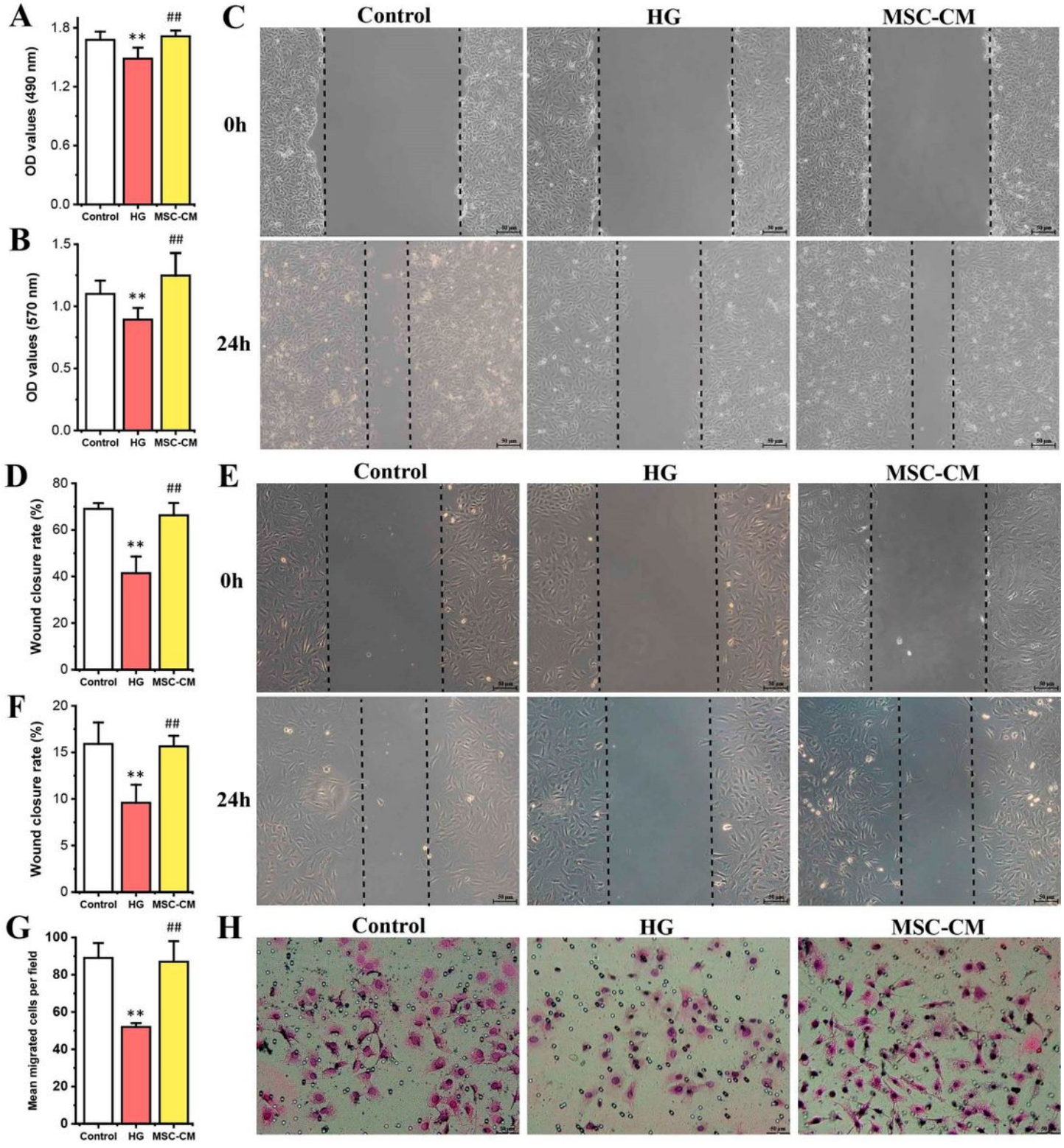

Figure 6

The effects of MSC-CM on the cell viability, wound healing and cell migration of HUVECs and HSFs in the control, HG and MSC-CM groups. (A) Cell viability of HUVECs was detected by MTT method. (B) Cell viability of HSFs was detected by MTT method. (C) and (D) showed wound closure rate and representative pictures in the scratch test of HUVECs (scale bar = 50 μm). (E) and (F) showed wound closure rate and representative pictures in the scratch test of HSFs (scale bar = 50 μm). (G) and (H)

showed the number of cell migration and the representative pictures of HUVECs in the transwell experiment (scale bar = 50 μm). Data were mean ± SD, $^{**}P < 0.01$ vs control level, and $^{\#\#}P < 0.01$ vs model level.

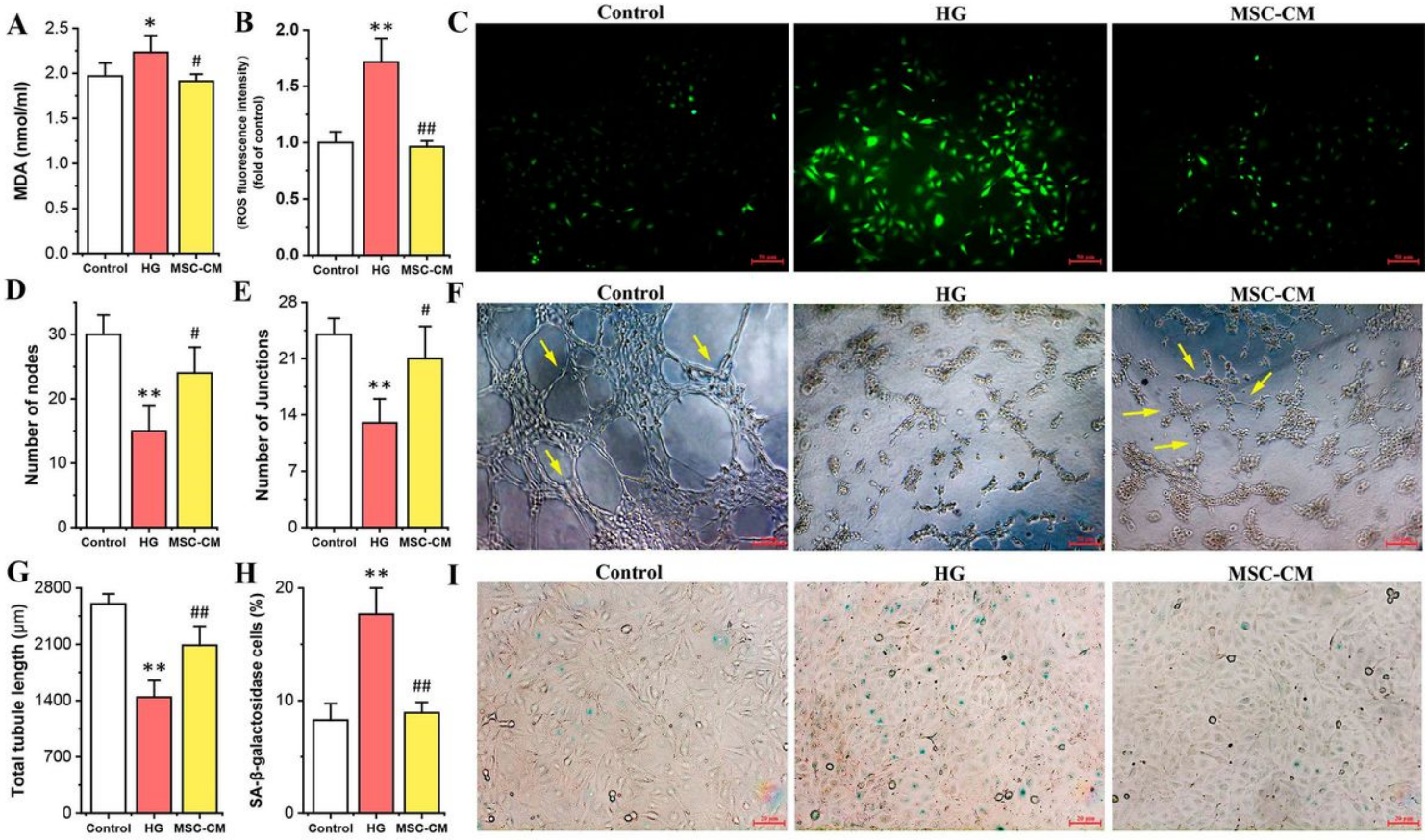

Figure 7

The effect of MSC-CM on oxidative stress, tubule formation and cell senescence in the control, HG and MSC-CM groups. (A) Malondialdehyde (MDA) measurement of HSFs. (B) and (C) showed that measurement and representative images of intracellular reactive oxygen species (ROS) levels of HSFs (scale bar = 50 μm). (D), (E), (F) and (G) showed that number of junctions, number of nodes, representative pictures, and total tubule length of tube networks calculated by Image-J software (scale bar = 50 μm). (H) and (I) showed that representative pictures with senescence cells after SA-β-galactosidase staining (scale bar = 20 μm). Data were mean ± SD, $^{*}P < 0.05$ and $^{**}P < 0.01$ vs control level, $^{\#}P < 0.05$ and $^{\#\#}P < 0.01$ vs model level.

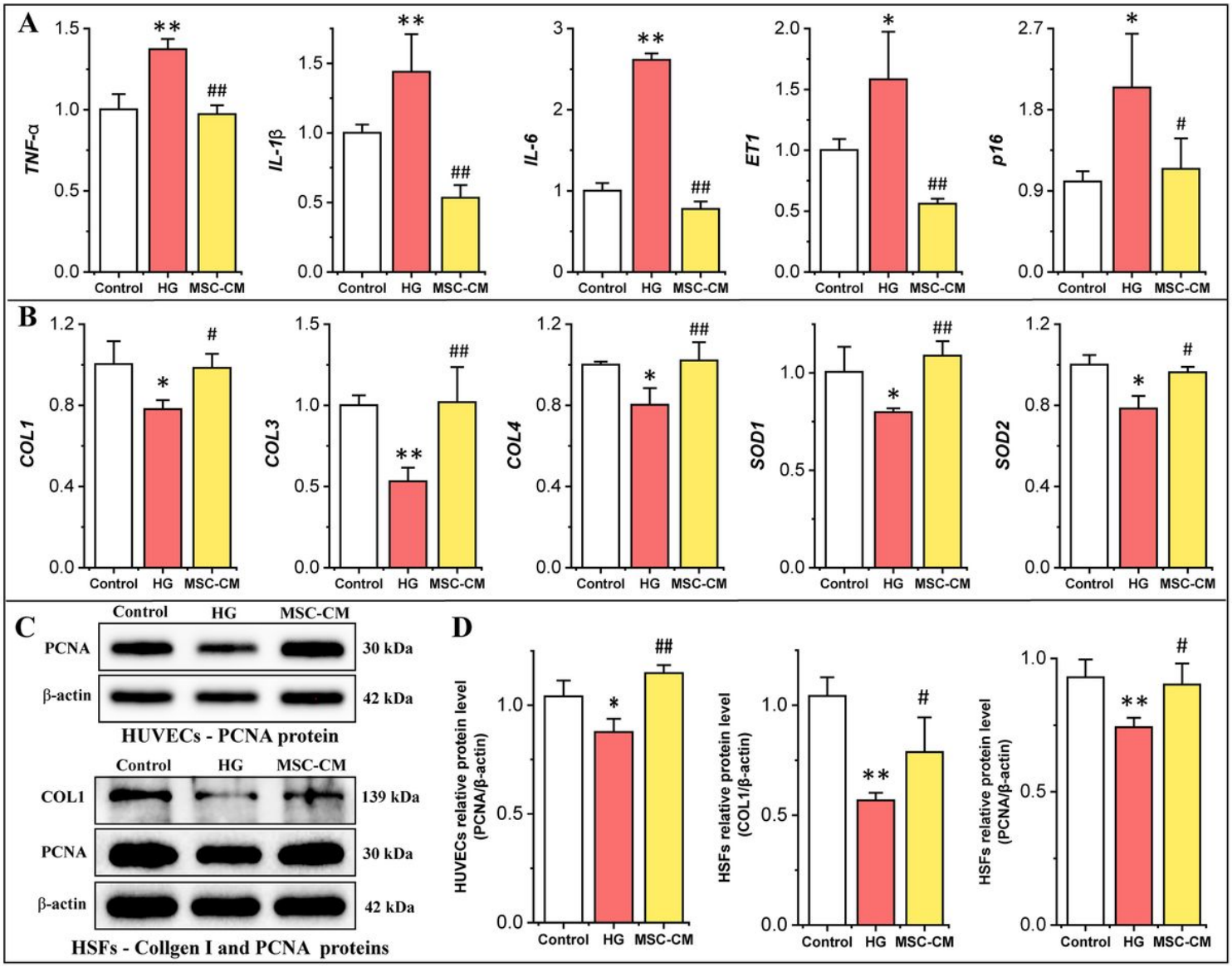

Figure 8

The role of MSC-CM treatment in mRNA and protein expressions of high glucose-induced HUVECs and HSFs. (A) mRNA expressions of inflammation (*TNF-α*, *IL-1β* and *IL-6*), tube formation (*ET-1*) and senescence (*p16*) related genes in HUVECs. (B) mRNA expressions of collagen synthesis (*COL1*, *COL3* and *COL4*), oxidative stress (*SOD1* and *SOD2*) related genes in HSFs. (C) Representative protein expression images of PCNA (HUVECs and HSFs) and COL1 (HSFs). (D) Relative protein levels of PCNA/β-ACTIN (HUVECs and HSFs) and COL1/β-ACTIN (HSFs). Data were mean ± SD, $^{*}P < 0.05$ and $^{**}P < 0.01$ vs control level, $^{\#}P < 0.05$ and $^{\#\#}P < 0.01$ vs model level.